Inferring the composition and concentration of aerosols by combining AERONET and MPLNET data: Comparison with other measurements and utilization to evaluate GCM output

Dilip Ganguly,[1,2] P. Ginoux,[1] V. Ramaswamy,[1,2] O. Dubovik,[3] J. Welton,[4] E. A. Reid,[5] and B. N. Holben[4]

Received 11 February 2009; revised 16 June 2009; accepted 23 June 2009; published 25 August 2009.

[1] In this work we demonstrate a method to derive the concentration of aerosol components from the spectral measurements of AOD (aerosol optical depth) and single scattering albedo along with their size distribution and extinction profile available from AERONET (Aerosol Robotic Network) and MPLNET (Micro-pulse Lidar Network) stations. The technique involves finding the best combination of aerosol concentration by minimizing differences between measured and calculated values of aerosol parameters such as AOD, single scattering albedo, and size distribution. We applied this technique over selected sites in three different regions of the United States (West coast, Great Plains, and North-East). Our results are then compared with the measured concentration of aerosol components available from IMPROVE (Interagency Monitoring of Protected Visual Environments) and EPA (Environmental Protection Agency) network, as well as two different versions of the GFDL (Geophysical Fluid Dynamics Laboratory) General Circulation Model AM2 with online and offline aerosols. In general, concentrations retrieved by our technique compare well with the ground-based measurements, but there are some discrepancies possibly due to the inherent differences in temporal and spatial scales of data averaging or some of the assumptions made in our study. Over continental North America, the online version of AM2 appears to overestimate sulfate concentration approximately by a factor of two and underestimate organic carbon by nearly the same amount. Results of our sensitivity study show that the errors in the retrieval of black carbon and sulfate concentrations could be as high as 100% when there is a large bias of $\sim$0.05 in the reference values of single scattering albedo under high AOD ($\geq$0.5 at 0.44 μm) conditions. Knowledge on the vertical distribution of aerosols is crucial for an accurate retrieval of surface concentration of aerosols. We also determine the composition and concentration of elevated aerosol layers using this technique.

Citation: Ganguly, D., P. Ginoux, V. Ramaswamy, O. Dubovik, J. Welton, E. A. Reid, and B. N. Holben (2009), Inferring the composition and concentration of aerosols by combining AERONET and MPLNET data: Comparison with other measurements and utilization to evaluate GCM output, *J. Geophys. Res.*, *114*, D16203, doi:10.1029/2009JD011895.

1. Introduction

[2] Aerosols play an important role in the radiation budget of the Earth-Atmosphere system by exerting direct and indirect forcing of climate [*Haywood and Boucher*, 2000]. Because of their short residence time and diverse aerosol types with varying optical properties, which are not uniformly distributed around the globe, aerosol radiative forcing exhibits large temporal and spatial differences [*Kiehl and Briegleb*, 1993; *Chung et al.*, 2005; *Forster et al.*, 2007]. Impacts of aerosols on climate are estimated using state of the art climate models which are able to reproduce the observed features of recent and past climate changes to a considerably good extent [*Forster et al.*, 2007]. These models have simulated global aerosol distribution with offline or online technique but involving some kind of model meteorology. However, a realistic and meaningful assessment of these impacts require an accurate distribution of aerosols in the model atmosphere. Thus it is crucial to evaluate model results globally by comparing them with observations.

[1]NOAA, Geophysical Fluid Dynamics Laboratory, Princeton, New Jersey, USA.
[2]Atmospheric and Oceanic Sciences Program, Princeton University, Princeton, New Jersey, USA.
[3]Laboratoire d'Optique Atmospherique, CNRS Universite de Lille, Villeneuve d'Ascq, France.
[4]NASA, Goddard Space Flight Center, Greenbelt, Maryland, USA.
[5]Aerosol and Radiation Modeling Section, Marine Meteorology Division, Naval Research Laboratory, Monterey, California, USA.

Copyright 2009 by the American Geophysical Union.
0148-0227/09/2009JD011895

[3] Only satellite instruments provide global coverage of aerosol optical depth and some information on their size distribution [*Kaufman et al.*, 2002]. Several researchers reported comparisons between satellite retrievals of aerosol optical depth (AOD) and those simulated by the global models [*Chin et al.*, 2002; *Penner et al.*, 2002; *Ginoux et al.*, 2006]. However, AOD is not generally the prognostic variable in global aerosol models, which actually predicts quantities like aerosol mass and number concentration. *Gassó and Hegg* [2003] introduced a scaling method to relate satellite products with the column integrated aerosol mass and compared their results with aircraft measurements. Subsequently, several studies tried to relate satellite derived AOD with near surface PM2.5 (particulate matter with aerodynamic diameter less than 2.5 μm) concentration for air quality monitoring purposes [*Wang and Christopher*, 2003; *Chu et al.*, 2003; *Liu et al.*, 2004, 2005; *Al-Saadi et al.*, 2005]. Most of these studies are based on some empirical relation derived from the regression analysis between the measurements of surface PM2.5 concentration and satellite derived AOD values. However, some recent studies emphasized on proper treatment of aerosol hygroscopicity and mixing state in satellite retrieval of AOD and its correlation with the estimation of PM2.5 concentration [*Wang and Martin*, 2007; *Shinozuka et al.*, 2007].

[4] So far, the composition of aerosols could not be retrieved through satellite measurements. Moreover, some of the key parameters controlling the direct and semidirect effect of aerosols such as single scattering albedo or the amount of absorption are still not available on a global scale and in a vertically resolved manner. This is important because the direct forcing due to absorbing aerosols like BC crucially depends on their presence above or below the cloud layer [*Haywood and Ramaswamy*, 1998]. Atmospheric heating at higher levels caused by absorbing aerosols could also result in the reduction of cloud amount through the semidirect effect [*Ackerman et al.*, 2000]. In this context, measurements made from the global network of AERONET and MPLNET stations are useful in retrieving some of these missing informations. *Dubovik et al.* [2002] developed an inversion algorithm to retrieve the major optical properties of aerosols from AERONET observations. Subsequently, *Schuster et al.* [2005] inferred the black carbon column content and specific absorption of aerosols from AERONET retrievals. However, these do not include detailed chemical properties of aerosols (i.e., aerosol composition) and are not vertically resolved. On the other hand, *Welton et al.* [2000] resolved optical properties vertically but only for the extinction coefficient and by assuming a constant lidar ratio. Raman lidars provide more information than backscatter lidar systems, but there are separate challenges and limitations associated with them [*Mattis et al.*, 2004].

[5] In this paper, we present a method which combines the AERONET and MPLNET data sets to derive the vertical distribution of aerosol composition from the spectral measurements of AOD and single scattering albedo along with their size distribution and extinction profile. In section 2, we explain our motivation beyond this work. Relevant aspects of the Geophysical Fluid Dynamics Laboratory (GFDL) Atmospheric General Circulation Model AM2, used to compare our results are described in section 3. The AERONET, MPLNET as well as data sets from two other aerosol monitoring networks in the United States are described in section 4. Section 5 presents the details of our methodology. Application of our technique over selected sites of United States are discussed in section 6. Comparisons of our results with the ground based measurements available from IMPROVE and EPA stations as well as two different versions of GFDL-AM2 model are presented in section 7. In section 8, we discuss the results of various sensitivity tests carried out to asses the effect of uncertainties associated with important parameters on the retrieval accuracy of our technique. Finally, our conclusions are presented in section 9.

2. Motivation

[6] From the modeling point of view, one wants to compare the simulated distribution of AOD with observations, understand the origin of any discrepancy for size distribution or optical properties of aerosols and correct them by tuning appropriate parameters or emission rates used in the model. Figure 1 shows the distributions of monthly mean AOD at 0.5 μm for July 2003 and January 2004 over the North American region as simulated by the GFDL Atmospheric General Circulation Model AM2 with online aerosols. Average values of AOD measured over the three AERONET sites corresponding to the same wavelength and for the same months are also shown in Figure 1 as solid circles with same color coding as the background plot depicting the model AOD. This comparison shows that under clear sky conditions, the model largely overestimates the observed AOD over this region. Even in the United States, there are very few places where we could analyze the origin of this discrepancy by comparing concurrently measured data for aerosol size distribution, their optical properties and mass concentration. This work is an attempt to fill this gap by combining different data sets and performing an objective analysis to extract all the parameters which could be used to constrain the model. Also, from the observational point of view, one would like to test the retrieval assumptions used in AERONET and MPLNET program by comparing different data sets to verify the physical consistency of all derived quantities. Both these factors have been the motivation of our present work.

3. GFDL-AM2 Model Description

[7] We compare the concentration of major aerosol components inferred using our method with those simulated by the GFDL Atmospheric General Circulation Model AM2 [*GFDL Global Atmospheric Model Development Team*, 2004] with online aerosols. This version of AM2 simulates major tropospheric aerosol types, such as sulfate, dust, OC (Organic Carbon), BC (Black Carbon) and sea salt. The model includes the following modules for aerosol simulation: emission, which includes sulfur, dust, black carbon, organic carbon, and sea salt emissions; chemistry, which currently uses a prognostic equation for H_2O_2 with prescribed OH, HO_2, O_3, and NO_3 fields simulated with MOZART-2 [*Horowitz et al.*, 2003] for gaseous sulfur oxidations; advection, which is computed by a semi-Lagrangian method; boundary layer turbulent mixing; moist convection [*GFDL GAMDT*, 2004]; dry deposition, which includes gravitational

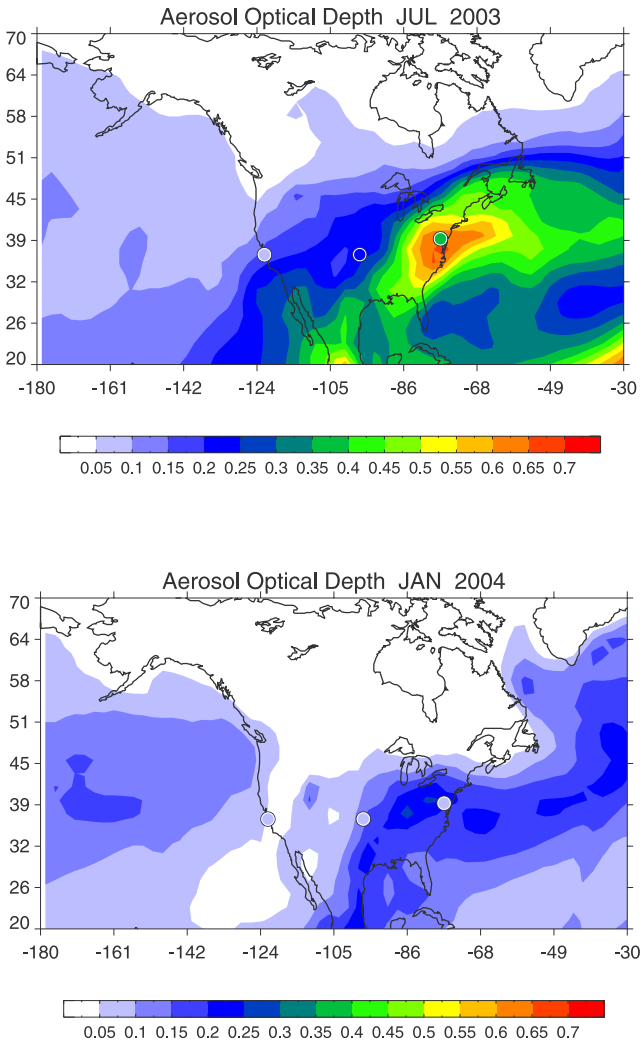

Figure 1. Monthly mean distribution of AOD at 0.5 μm for July 2003 and January 2004 over the North American region as simulated by the GFDL atmospheric general circulation model (AM2) with online aerosols. Measured values of AOD at the three AERONET sites and corresponding to the same wavelength are also shown as solid circles with same color coding as the background plot depicting the model AOD.

settling as a function of aerosol particle size, hygroscopicity and air viscosity [*Chin et al.*, 2002] and surface deposition as a function of surface type and meteorological conditions [*Wesely*, 1989; *Li et al.*, 2008]; and wet deposition, which accounts for the scavenging of soluble species in convective updrafts and rainout/washout in large-scale precipitation [*Giorgi and Chameides*, 1986; *Balkanski et al.*, 1993].

[8] Sulfate aerosols are mostly formed by oxidation of SO_2 emitted from fossil fuel combustion. Sulfur dioxide fossil fuel emissions are based on energy statistics for the year 2000 as described by *Dentener et al.* [2006]. In order to account for the SO_2 emissions from biomass burning sources, we use the monthly data for large-scale fire emissions based on the Global Fire Emission Database (GFED) inventory [*Van derWerf et al.*, 2006]. In addition to direct emission, SO2 is produced from the oxidation of dimethylsulfide (DMS) released from the ocean. DMS emission is based on the parameterization proposed by *Chin et al.* [2002]. The carbonaceous aerosols emission from biomass burning is based on GFED monthly data, while annual emission from biofuel and fossil fuel burning are based on the inventory for the year 2000 developed by *Dentener et al.* [2006]. Secondary organic aerosol (SOA) formed by the oxidation of volatile organic compounds are also simulated and are assumed to result from the oxidation of α-pinene ($C_{10}H_{16}$) and n-butane (C_4H_6). We use the same reaction rates as the ones proposed by *Tie et al.* [2005]. The BC emissions from both fossil fuel and biomass burning are assumed to occur as 80% hydrophobic and 20% hydrophilic, whereas OM (Organic Matter) emissions occur as 50% hydrophobic and hydrophilic. The aging of carbonaceous aerosols are treated as in the work of *Reddy and Boucher* [2004] with an exponential lifetime of 1.63 days. Dust emission follows the parameterization of *Ginoux et al.* [2001], and is based on the preferential location of sources in topographic depression. Sea salt particles are emitted from the ocean according to *Monahan et al.* [1986].

[9] In AM2, sulfate aerosols are considered to be optically equivalent to ammonium sulfate and their refractive indices as a function of RH as well as their mass growth factors are inherited from the work by *Tang and Munkelwitz* [1994]. For organic aerosols, growth factors are obtained from the work of *Ming and Russell* [2004] while their refractive indices are taken from the work of *Hess et al.* [1998]. In the case of sea salt aerosols, refractive indices and growth factors are both inherited from the work of *Tang et al.* [1997]. Black carbon and dust aerosols are assumed to be hydrophobic, and their properties are considered as independent of relative humidity. Optical properties of dust and black carbon aerosols are taken from the works of *Balkanski et al.* [2007] and *Haywood and Ramaswamy* [1998] respectively. We assume spherical properties of all aerosols, which may not be valid for freshly emitted dust. However, as our selected sites are far from any major source of dust, the errors associated with nonspherical particles should be negligible. Mass density of wet particles are estimated as the volume-weighted density of dry aerosol and water.

[10] The model has a resolution of 2° latitude × 2.5° longitude with 24 vertical levels (on a η coordinate system). The model is driven by the observed monthly mean sea-surface temperature values. The dynamical fields are nudged toward the NCEP (National Center for Environmental Prediction) reanalysis using a relaxation method, with the relaxation timescale being 6 hour [*Moorthi and Suarez*, 1992]. This procedure ensures that the models meteorology mimics as best as possible the present-day known patterns.

4. Data Sets

[11] In our study, we use observational data from multiple sources to retrieve the composition and concentration of aerosols over specific locations. Major aerosol parameters used in our analysis include the spectral values of AOD and single scattering albedo along with the size distribution and the extinction profile of aerosols in the atmosphere. Data on

AOD, single scattering albedo and the size distribution of aerosols are obtained from the AERONET global network, while the extinction profile of aerosols is obtained from the MPLNET program.

[12] This section presents a brief description of all input data sets used in our analysis, along with other data sets used to compare the results of our retrieval.

4.1. AERONET Data

[13] The first data set to be used in the present analysis consists of AOD from AERONET sites, measured using CIMEL Sun/sky radiometers [*Holben et al.*, 1998, 2001]. AERONET is a federated worldwide network of Sun Photometers that are monitored and maintained at the NASA Goddard Space Flight Center [*Holben et al.*, 1998]. In our analysis, we have used the monthly mean values of AOD at 0.34, 0.38, 0.44, 0.5, 0.675, 0.87 and 1.02 μm. *Holben et al.* [2001] reported a total uncertainty $\sim$0.01–0.03 in the estimated values of $\tau(\lambda)$, which is spectrally dependent with higher errors in the near ultraviolet than in visible range.

[14] Two additional parameters used in our analysis viz. the size distribution of aerosols and their single scattering albedo (ω) are also obtained from AERONET measurements but after inversion of almucantar data [*Dubovik and King*, 2000]. The AERONET inversion algorithm retrieves aerosol size distribution for 22 size bins between 0.05 and 15 μm and single scattering albedo at four wavelengths viz. 0.44, 0.67, 0.87 and 1.02 μm. According to *Dubovik et al.* [2002], the accuracy level in the retrieval of single scattering albedo is of the order of 0.03 for high aerosol loading (AOD at 0.44 μm $\geq$ 0.5) and for solar zenith angle >50°. However, for low aerosol loading (AOD at 0.44 μm $\leq$ 0.2), the accuracy level could drop down to 0.05. Similarly, *Dubovik et al.* [2000] have also shown that errors involved in the retrieval of volume size distribution are a nonlinear function of particle size, aerosol type and the actual values of $dV(r)/dlnr$. In particular, the retrieval errors do not exceed 10% for $0.1 \leq r \leq 7$ μm but may increase up to 80% at the edges of the distribution ($0.05 \leq r \leq 0.1$ μm and $7 \leq r \leq 15$ μm). However, these errors at the edges do not significantly effect the important characteristic features of the distribution. From the size distribution of aerosols, quantities which are actually used for comparison in our analysis are the total volume fraction of fine (C_{vf}) and coarse (C_{vc}) mode particles, calculated according to the following relation

$$C_v = \int_{r_{\min}}^{r_{\max}} \frac{dV(r)}{dlnr} dlnr \tag{1}$$

[15] It has to be mentioned here that in the older version of AERONET products (Version 1), the separation radius (r_{sp}) between C_{vf} and C_{vc} was fixed at 0.6 μm. However, in the latest version (Version 2) of data used in our analysis, this separation radius is flexible and a program is used to search the minima of size distribution between 0.194 μm and 0.576 μm to separate the two size modes. In our analysis, we use only quality assured Level 2 (of Version 2) data for AOD. However, in the case of inversion products like size distribution and single scattering albedo, we resort to Level 1.5 data (cloud screened but not necessarily quality assured data from Version 2) whenever the corresponding Level 2 data are not available.

4.2. MPLNET Data

[16] Another important data set used in the present study is the vertical distribution of aerosols obtained from MPLNET (comprised of a network of ground-based backscatter lidar systems) stations which are collocated with Sun/sky radiometer sites of AERONET network [*Welton et al.*, 2001]. MPLNET provides time series of extinction profiles at green wavelengths (0.523, 0.527, or 0.532 μm) from its measurement locations. Raw MPLNET data consist of profiles of attenuated backscatter photon counts acquired at 1 minute temporal and 75 meters vertical resolutions, continuously, up to an altitude of 60 km (30 km is maximum range for profiling). These raw data are subjected to several correction procedures such as dead time correction, after pulse correction, overlap correction etc. to finally retrieve the extinction profile of aerosols, following the detailed algorithm described by *Campbell et al.* [2002] and *Welton and Campbell* [2002]. During this process, extinction profiles from MPLNET are normalized to match the estimated AOD at the lidar wavelength. The estimated AOD is derived by applying the polynomial fit method of *Eck et al.* [1999] to the AOD values over a range of wavelengths measured by AERONET. Errors in retrieved extinction profiles are calculated from measured signal and AOD uncertainties, and are greater when the AOD is low. *Schmid et al.* [2006] has shown that the accuracy of MPLNET aerosol products are typically within 20%. It has to be mentioned here that the extinction data from one of the stations (CART site) used in this study is a part of Atmospheric Radiation Measurement (ARM) program but processed using the MPLNET algorithm. All MPLNET data used here are Level 1.5 (Version 2) which are cloud screened following the AERONET procedure developed by *Smirnov et al.* [2000].

4.3. IMPROVE Data

[17] In order to validate the results of our technique, we compare the concentrations of individual aerosol components retrieved by this method with the actual measured surface concentrations of aerosols obtained from the IMPROVE (Interagency Monitoring of Protected Visual Environments) data set. IMPROVE program has collected aerosol samples twice weekly starting from 1988 at almost 200 sites located in National Parks of the United States [*Malm et al.*, 1994]. It is important to mention here that all concentration provided by the IMPROVE program are measured from PM2.5 (Particulate matter with aerodynamic diameter of less than or equal to 2.5 μm) aerosol samples. Main aerosol components measured under this program include $SO_4^{=}$, OC (organic carbon), BC (black carbon) and submicron dust particles. In this work we use the monthly mean climatological concentrations of different aerosol species.

4.4. EPA Data

[18] We also compare our results with the concentration data available from the Speciation Trends Network (STN) maintained by EPA (Environmental Protection Agency of

Table 1. Microphysical Properties of Aerosol Components in Dry State[a]

Component	σ (μm)	r_{modN} (μm)	r_{modV} (μm)	ρ (g/cm^3)
Sulfate (Slf)	2.0	0.05	0.17	1.77
Black carbon (BC)	1.8	0.04	0.095	1.0
Organic carbon (OC)	1.49	0.085	0.126	1.8
Small dust (Ds1)	2.0	0.38	1.26	2.5
Large dust (Ds2)	1.6	2.6	4.517	2.6
Sea salt accumulation (SS1)	1.59	0.13	0.22	2.16
Sea salt coarse (SS2)	2.0	0.74	2.46	2.16

[a]Here the size parameters σ (width of the distribution), r_{modN} (mode radius for number size distribution) and r_{modV} (mode radius for volume size distribution) correspond to lognormal size distribution of aerosols and ρ is the mass density of aerosol particles.

United States) for PM2.5 aerosol samples. The STN consists of 54 core sites and about 200 supplemental State and Local Monitoring Stations (SLAMS) across the United States. The monitoring schedule of EPA consists of 24-hour average measurements (starting at midnight) every third day (at a majority of sites) or every sixth day (at a few sites). Most monitors under EPA program measure a standard set of data, including PM2.5 mass and its composition in terms of major aerosol species like sulfate, nitrate, ammonium, organics, and elemental carbon [*Solomon et al.*, 2001].

5. Methodology

[19] The method developed to derive the aerosol composition over any location is equivalent to a minimization technique. The first step is to compute a discrete number of optical properties for individual aerosol components such as their mass extinction efficiency, single scattering albedo and asymmetry parameter at desired wavelengths and corresponding to various relative humidity conditions using a Mie code [*Bohren and Hoffman*, 1998]. In our analysis, we used seven aerosol components viz. sulfate (Slf), black carbon (BC), organic carbon (OC) and two size bins each of dust (DS1, DS2) and sea salt (SS1, SS2). Table 1 summarizes the microphysical properties of all the aerosol components used in this study. Here the size distribution parameters of all aerosol components except organic carbon are obtained from AEROCOM (Aerosol Comparisons between Observations and Models) project (see http://nansen.ipsl.jussieu.fr/AEROCOM/ [*Textor et al.*, 2006]). For organic carbon, we obtain the size parameters from *Ming et al.* [2005]. The second step consists of constructing the concentration profiles of individual aerosol components according to the observed profiles of aerosol extinction from MPLNET measurements. This is followed by calculation of values for parameters like AOD (τ), single scattering albedo (ω), volume fraction of fine (C_{vf}) and coarse (C_{vc}) mode particles for numerous possible mixtures (assuming external mixture) of aerosol components with varying mass concentrations. Finally, the last step is to determine the most optimum combination of aerosol concentration which simultaneously minimizes the difference between observed and computed values of all these parameters.

5.1. Optical Properties of Individual Aerosols

[20] The extinction coefficient $\beta_{i_{ext}}(\lambda, z)$ of any aerosol component i at altitude level z and corresponding to wavelength λ can be expressed according to the relation

$$\beta_{i_{ext}}(\lambda, z) = C_{i_{amb}}(z)\sigma_{i_{ext}}(\lambda, z) = C_{i_{dry}}(z)G_i(z)\sigma_{i_{ext}}(\lambda, z) \quad (2)$$

where $C_{i_{amb}}(z)$ and $C_{i_{dry}}(z)$ are the ambient and dry mass concentrations (μg.m^{-3}) respectively, $G_i(z)$ is the mass growth factor and $\sigma_{i_{ext}}(\lambda, z)$ is the mass specific extinction cross section (m^2 g^{-1}) of the corresponding aerosol under relative humidity (RH) conditions prevailing at level z. It has to be mentioned here that growth factor and mass specific extinction cross section of aerosol components are actually functions of RH, which in turn varies with altitude; hence both these parameters are expressed as a function of vertical level z. In our analysis, we use the same refractive indices and mass growth factors of individual aerosol components as in AM2 (see section 3) to compute various optical properties like extinction coefficient and single scattering albedo using Mie theory. Altitude profiles of relative humidity obtained from NCEP reanalysis data are used to compute the hygroscopic growth factors of individual aerosol components and corresponding changes in their physical and optical properties at all vertical levels.

5.2. Construction of Concentration Profiles

[21] Since equation (2) is valid throughout the atmosphere, it is possible to relate the aerosol concentration for different levels as

$$C_{i_{dry}}(z+1) = C_{i_{dry}}(z)\frac{\beta_{i_{ext}}(\lambda, z+1)\sigma_{i_{ext}}(\lambda, z)G_i(z)}{\beta_{i_{ext}}(\lambda, z)\sigma_{i_{ext}}(\lambda, z+1)G_i(z+1)} \quad (3)$$

where $C_{i_{dry}}(z = 0)$ is the unknown concentration that we are trying to estimate. An important assumption made here is that the contribution of individual aerosol components to the total extinction remains the same at all vertical levels such that

$$\frac{\beta_{i_{ext}}(\lambda, z+1)}{\beta_{i_{ext}}(\lambda, z)} = \frac{\sum_{i=1}^{n}\beta_{i_{ext}}(\lambda, z+1)}{\sum_{i=1}^{n}\beta_{i_{ext}}(\lambda, z)} \quad (4)$$

where n is the total number of aerosol components present in the atmosphere. Since the total extinction due to all aerosol components corresponds to lidar measurements, we may write

$$\left.\frac{\beta_{i_{ext}}(z+1)}{\beta_{i_{ext}}(z)}\right|_{\lambda=0.52\mu\mathrm{m}} = \frac{\beta_{ext}^{mpl}(z+1)}{\beta_{ext}^{mpl}(z)} \quad (5)$$

where $\beta_{ext}^{mpl}(z)$ and $\beta_{ext}^{mpl}(z + 1)$ represents the extinction coefficient of aerosols measured by the lidar system corresponding to levels z and $z + 1$ respectively. Our assumption here is similar to choosing a constant lidar ratio for all vertical levels (ratio of extinction to backscattering coefficient of aerosols), which is a common assumption in backscatter lidar inversion algorithms [*Welton et al.*, 2000]. Our assumption is generally valid when (1) the majority of

aerosols are confined within the well mixed boundary layer of the atmosphere, (2) most of the aerosols over any location are locally produced and (3) and there are no major elevated aerosol layers (due to long range transport), contributing significantly to the columnar AOD and other aerosol parameters. Thus using equations (3) and (5), we construct the concentration profiles of all aerosol components. In case there are distinct aerosol layers in the atmosphere, we assume that each of these aerosol layers are independently well mixed within itself. Under such conditions, we consider our earlier assumption in the form of equation (4) to remain valid within each layer. However, such cases must be treated very carefully due to some restriction as discussed with an example in section 6.2.2.

5.3. Optical Properties of Aerosol Mixture

[22] Assuming external mixture and lognormal size distributions of aerosol components, we now successively calculate the optical depth, single scattering albedo and the volume fraction of fine and coarse modes particles. AODs for individual aerosol components are estimated by integrating the vertical profiles of extinction coefficient for respective components as

$$\tau_i(\lambda) = \int_{z=0}^{H} \beta_{i_{ext}}(\lambda, z)dz \tag{6}$$

where H is the maximum vertical level up to which lidar data is available (usually more than 10 km above the ground level). Total AOD due to all aerosols is obtained as the sum of contributions by individual components such that

$$\tau(\lambda) = \sum_{i=1}^{n} \tau_i(\lambda) \tag{7}$$

where $\tau_i(\lambda)$ and $\tau(\lambda)$ are the AOD fraction due to a particular component and the total AOD at wavelength λ respectively. Single scattering albedo for a mixture of n aerosol components is computed according to the relation

$$\omega(\lambda) = \frac{\sum_{i=1}^{n} \tau_i(\lambda)\omega_0(i, \lambda)}{\tau(\lambda)} \tag{8}$$

where $\omega_0(i, \lambda)$ and $\omega(\lambda)$ are the single scattering albedo for a single component and for all components respectively at wavelength λ. Size distribution for the total (i.e., vertically integrated) aerosol loading is obtained by adding lognormal distributions of each aerosol component according to the following expression

$$\frac{dV(r)}{dlnr} = \sum_{i=1}^{n} \frac{V_i}{\sqrt{2\pi}\ln\sigma_i} \exp\left[-\frac{\ln^2\left(\frac{r}{r_{mi}}\right)}{2(\ln\sigma_i)^2}\right] \tag{9}$$

where V_i is the total volume, r_{mi} is the mean radius and σ_i is the geometric standard deviation corresponding to the lognormal distribution of a particular aerosol component. The volume fraction of fine ($0.05 < r < r_{sp}$ μm) and coarse ($r_{sp} < r < 15$ μm) mode particles are calculated according to equation (1) by integrating the volume size distribution within specified limits as explained in section 4.1.

5.4. Minimization Process

[23] Once all parameters viz. $\tau(\lambda)$, $\omega(\lambda)$, C_{vc} and C_{vf} are estimated for a particular combination of aerosol concentration, we define a quantity ϕ representing the difference between the aerosol model and observations as

$$\phi^2 = \frac{1}{M}\sum_{i=1}^{M} \frac{\left(X_i^m - X_i^o\right)^2}{\epsilon_i^2} \tag{10}$$

where X_i^o and X_i^m are the observed and computed values of aerosol parameter respectively and the sum is over total number (M) of variables used for comparison. In the present case M is equal to 13 with contributions of 7, 4, 1 and 1 corresponding to $\tau(\lambda)$, $\omega(\lambda)$, C_{vc} and C_{vf} respectively. The normalization ϵ_i^2 corresponds to the square of uncertainties associated with each parameter. Use of this weighting factor makes sure that the terms corresponding to different parameters in equation (10) are of comparable order and more accurate observations makes larger contribution to the quantity ϕ^2. Since the current version of AERONET data (Version 2) does not provide exact error estimates for every single measurement, we used the general uncertainties associated with each parameter as reported by *Dubovik et al.* [2000]. For AOD, we assume an absolute uncertainty of ± 0.01 for $\lambda \geq 0.44$ μm and ± 0.02 for $\lambda < 0.44$ μm. In the case of single scattering albedo, we assume a general uncertainty of ± 0.03 at all the four wavelength channels for which data is available. Similarly, in the case of size distribution, we assume a relative uncertainty of 60% in both C_{vf} and C_{vc}. Nevertheless, in order to understand the effect of various uncertainties associated with different parameters on the retrieval of aerosol concentration using this method, we carried out various sensitivity tests which are discussed in section 8.

[24] The minimization process starts with some initial guess concentrations. Then the entire procedure starting from the choice of this initial concentration is repeated for a range of aerosol models and finally, the one corresponding to the lowest ϕ^2 is selected. As a first guess, initial concentration of aerosol components are estimated by trial and error method. Some concentrations are assumed for each aerosol component and a comparison is made between observed and computed values of parameters under ambient relative humidity conditions. Subsequently, this process is repeated for every aerosol model in the minimization loop. In order to increase the accuracy of final solution and fine tune the concentration of individual components, the minimization process is iterated. We found that two stage iteration were sufficient for our purpose.

6. Application Over Different Sites

[25] The method described above is applied over three different sites in United States viz. GSFC (Goddard Space Flight Center) in Maryland, Cart Site in Oklahoma and Monterey in California where there are close to one year of concurrently measured data available for parameters like AOD, single scattering albedo, size distribution and vertical profile of aerosols which are all required for this technique. Another reason for selecting these North American sites is that here it was possible to compare the near surface aerosol

Table 2. Month and Year of Data From Different Sites Used in This Study

Year	GSFC (39 N, 76.8 W)	Cart Site (36.6 N, 97.5 W)	Monterey (36.6 N, 121.9 W)
2000	–	June – September	–
2002	January – October	February – May	–
2003	November – December	–	April – October

concentrations retrieved by our technique with the ground based measurements available from these regions. Table 2 lists the months and years of data from the three sites used in this study. In this section we discuss the observed characteristics of major aerosol parameters over these three sites and their comparison with computed values based on the results of our minimization.

6.1. GSFC Site

[26] Considering the location of the GSFC site, we used all seven aerosol components including the two modes of sea salt aerosols in our analysis. We used quality assured Level 2 data for AOD and size distribution of aerosols. However, in the case of single scattering albedo, Level 2 data were available only for July, September and October, so we resorted to using Level 1.5 data for other months. We now discuss the comparison between observed and computed values of different aerosol parameters from this particular site.

6.1.1. AOD and Single Scattering Albedo

[27] Figure 2 shows the comparison between observed and computed values of parameters like AOD, single scattering albedo, vertical profile and the size distribution of aerosols based on the results of our minimization for two selected months of the year 2002. From Figures 2a and 2d, AOD values at all wavelengths are almost an order of magnitude higher in July than in January. Higher AOD during summer is associated with higher aerosol loading. However, the observed increase in AOD is not necessarily accompanied by a simultaneous increase in surface concentration of aerosols as, during summer months, aerosols are spread over a large volume of the atmosphere (discussed in the next section). Table 3 gives the list of monthly mean values of AOD at 0.5 μm based on the results of our minimization, measurements available available from the three AERONET sites and those simulated by the AM2 model for the corresponding periods mentioned in Table 2. In general, AOD values are overestimated in AM2 simulations during all months (especially during winter season) and over all sites. *Ginoux et al.* [2006] attributed this discrepancy to hygroscopicity of aerosols which is overestimated by the model. In our minimization, computed values of AOD at all wavelengths are ensured to lie within a difference of ±0.03 with respect to their measured values, which is the maximum uncertainty in AOD for Level 1.5 data at any AERONET site as reported by *Holben et al.* [2001].

[28] A concurrent increase in single scattering albedo from January to July indicates an increase in relative dominance of scattering aerosols during summer months. On the other hand, lower values of single scattering albedo during January than in July shows the relative dominance of absorbing aerosols during winter months. Main absorbing species which can lower the single scattering albedo of aerosols are BC and soil dust. Interestingly, both these components exhibit different characteristics in their wavelength dependency of absorption. Lower values of single scattering albedo in the near infrared wavelengths compared to visible range indicates the dominance of BC aerosol during January as it exhibits stronger absorption characteristics in the near infrared range [*Bergstrom et al.*, 2002]. Dust aerosols on the other hand absorb more strongly in the near ultra violet region as compared to visible or near infrared region due to presence of iron oxides in the form of hematite [*Balkanski et al.*, 2007]. Single scattering albedo values during July are high and exhibit less wavelength dependency, indicating a stronger role played by scattering type aerosols in summer season. Our result suggests that the noted increase in single scattering albedo is mainly due to an increase in the ratio of sulfate to BC mass, which increased by almost an order of magnitude from ~1.5 in January to nearly 16 in July, and partly because the OC concentrations also increased by nearly 1.5 times over the same period. However, we believe that the observed decrease in wavelength dependency of single scattering albedo is mostly due to increase in sulfate to BC mass ratio from January to July. IMPROVE data also shows an increase in sulfate to BC mass from around4 in January to nearly 13 in July. The effect of possible errors associated with single scattering albedo on the retrieval of aerosol concentrations using this technique are discussed separately in a following section.

6.1.2. Extinction Profile

[29] Figures 2b and 2e shows the monthly mean profiles of aerosol extinction coefficient from lidar measurements for the months of January and July 2002. These plots also show the extinction profiles for individual aerosol components and the total extinction due to all components corresponding to the best combination of aerosol concentrations estimated by our technique. As the lidar profile shows, extinction values at all altitudes are much lower in January as compared to July. The January and July profiles are typical for winter and summer season respectively. During winter months, most aerosols remain confined within a shallow boundary layer extending up to about 1 km from the surface. Beyond this level, aerosol concentration decreases sharply with increase in altitude and extinction values become almost nil above 2.5 km. On the other hand, extinction profiles for summer months are characterized by a thick aerosol layer extending from the surface up to 4 km altitude. Extinction profiles during other months are somewhat intermediate between the profiles of January and July.

[30] An important factor influencing the extinction coefficient of many aerosol species is the relative humidity in the atmosphere. The maroon line in both Figures 2b and 2e represents the monthly mean profile of relative humidity over this site obtained from NCEP reanalysis data for the months of January and July respectively. It can be seen from Figure 2 that although relative humidity values close to the surface are higher during January, it decreases sharply above 0.75 km and remains below 60% mark at further higher levels. On the other hand during July, although RH values are relatively low near the surface, it increases to reach a maxima of about 75% at around 1.5 km. Most

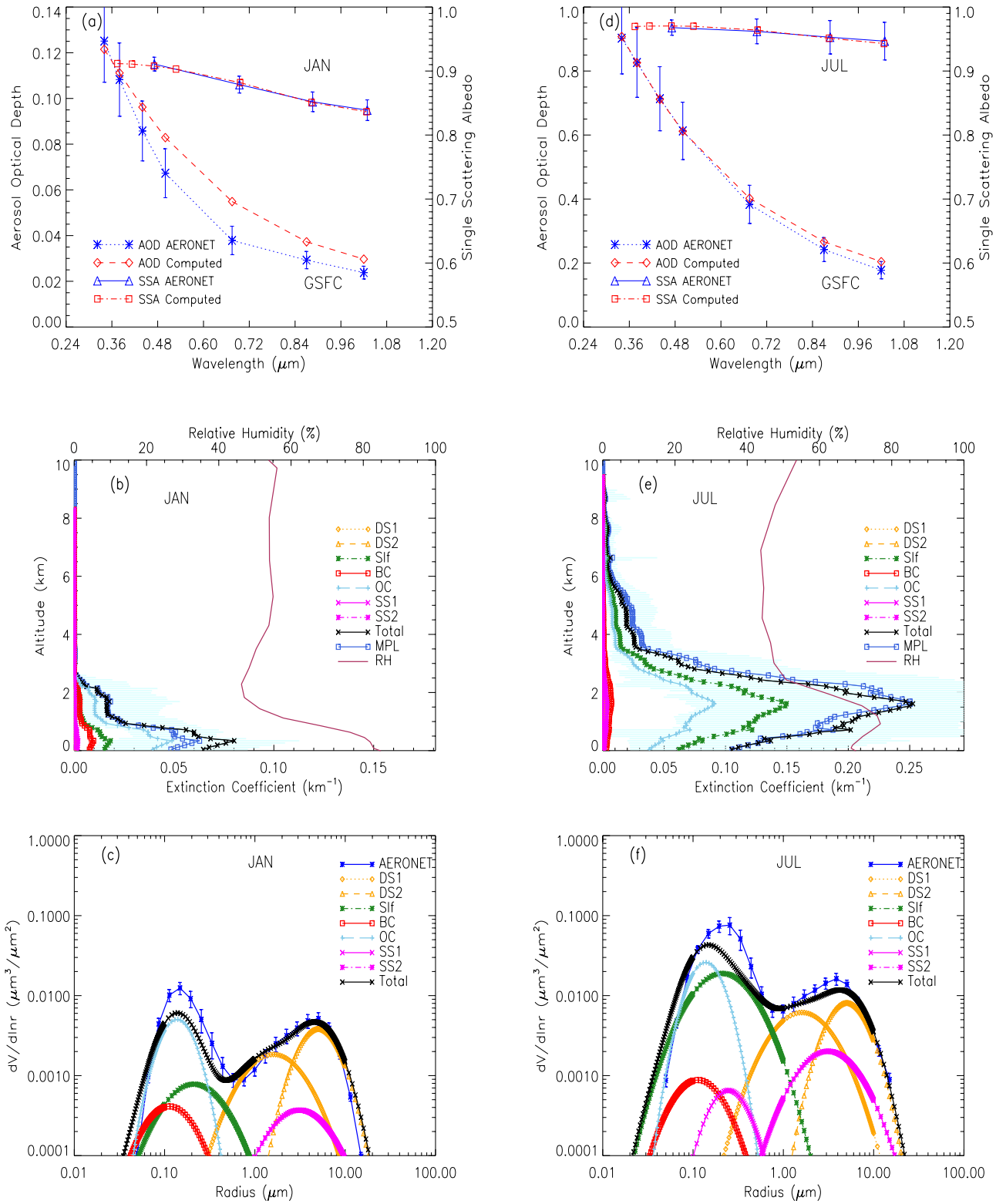

Figure 2. Comparison of AOD, single scattering albedo (SSA), extinction profile and the size distribution of aerosols for January and July 2002 corresponding to the AERONET/MPLNET observations from GSFC with their estimated values based on our minimization. Vertical lines in Figures 2a, 2c, 2d, and 2f represent the standard error about the mean value of the corresponding parameter during the respective month. Profiles corresponding to MPL in Figure 2b and 2e represent the extinction coefficients from MPLNET and horizontal lines represent the standard deviation in this data at various altitudes. Maroon line in Figures 2b and 2e represents the monthly mean profile of relative humidity from NCEP reanalysis.

Table 3. Comparison of Monthly Mean AOD at 0.5 μm Over the Three Selected Sites Based on the Results of our Minimization With the Measured Values Available From AERONET and Those Simulated by the AM2 Model Corresponding to the Periods Mentioned in Table 2

	GSFC			Cart Site			Monterey		
Month	Minz	AERONET	AM2	Minz	AERONET	AM2	Minz	AERONET	AM2
January	0.08	0.07	0.22			0.13			0.06
February	0.10	0.09	0.25	0.09	0.07	0.16			0.04
March	0.17	0.15	0.35	0.12	0.11	0.23			0.05
April	0.21	0.18	0.39	0.17	0.15	0.19	0.11	0.10	0.06
May	0.29	0.26	0.60	0.22	0.19	0.35	0.14	0.13	0.04
June	0.45	0.44	0.75	0.16	0.16	0.38	0.14	0.13	0.04
July	0.61	0.61	0.64	0.19	0.18	0.23	0.10	0.09	0.17
August	0.43	0.41	0.87	0.24	0.23	0.49			0.16
September	0.24	0.24	0.50	0.19	0.18	0.35	0.11	0.09	0.09
October	0.22	0.20	0.35			0.28	0.08	0.07	0.04
November	0.07	0.10	0.44			0.16			0.05
December	0.07	0.06	0.16			0.13			0.06

importantly, RH values during July remain above 60% mark at all levels from the surface to about 3 km in the atmosphere. This results in increasing the extinction efficiency of hygroscopic aerosols like sulfates and organics which contribute significantly to the total aerosol extinction between these two levels.

[31] Table 4 lists the percentage contribution of major aerosol components toward the total AOD during different seasons over the three selected sites based on the results of minimization. Our results show that organics contribute significantly (25–60%) to the annual mean AOD at 0.5 μm (all percentage contributions to AOD refereed hereafter are with respect to 0.5 μm). This is followed by sulfate aerosols whose contribution is maximum in July (65%) and minimum in December (16%). Interestingly, during summer months when sulfate aerosols contribute maximum to the AOD, contributions by organics are among its lowest. BC contribution peaks in winter months ($\sim$15%) and reaches minimum in summer ($\sim$4%). Although dust contributes significantly (30–60%) to the total aerosol mass concentration, its contribution to AOD is limited to $\sim$4% during July–August and $\sim$8% during April–May. Similarly, sea salt contribution to AOD is very small (2–5%) although its mass is not negligible.

6.1.3. Size Distribution

[32] Figures 2c and 2f shows the volume size distribution obtained from AERONET measurements over GSFC for the months of January and July 2002. Size distribution pattern for all months show the presence of two distinct modes corresponding to fine and coarse range particles with a separation point $\sim$0.5 μm radius. These plots also show the size distribution of individual aerosol components based on the results of our minimization in different colors along with the total size distribution due to all components in black. Major aerosol components contributing to the coarse mode size distribution include two modes of dust (Ds1 and Ds2) and one mode of sea salt (SS2) aerosol. On the other hand, fine mode fraction of aerosols consists of BC, OC, sulfate, one mode of sea salt (SS1) and some fraction of small dust (Ds1). We find the ratio of sulfate to OC mass to be higher during summer than in winter months. Volume fraction of small dust (Ds1) with respect to large dust (Ds2) aerosols are highest during spring (April–May) while their contributions are comparable during summer months. BC mass fraction in total aerosol loading is found to be higher during January compared to July. We may recall that although coarse mode particles have a larger contribution toward the mass loading, the maximum contribution to AOD comes from fine mode particles like sulfate and organics.

6.2. Cart Site and Monterey

[33] Two other sites where the current method is applied are Cart Site in Oklahoma and Monterey in California. For both these locations, we used Level 2 data for AOD and size distribution, and Level 1.5 data for single scattering albedo. Aerosol data needed for our technique are available for shorter periods from these two locations as compared to the GSFC site. In order to examine the seasonal variation of aerosol concentration over all chosen sites, we use the available data over several years. For the Cart Site, we used data from the years 2000 and 2002, while for Monterey, we used data from 2003 (see Table 2).

6.2.1. AOD and Single Scattering Albedo

[34] Figure 3 shows the comparison between observed data and computed values of major aerosol parameters based on the results of minimization for the months of

Table 4. Percentage Contribution of Major Aerosol Components Toward the Total AOD During Different Seasons Over the Three Selected Sites Based on the Results of our Minimization

Months	Dust	Sulfate	BC	OC	Sea Salt
		GSFC			
DJF	7	19	13	57	4
MAM	8	24	7	56	5
JJA	4	45	4	45	2
SON	5	40	4	46	5
		Cart Site			
DJF	26	16	21	37	
MAM	14	16	17	53	
JJA	13	31	5	51	
SON	15	19	3	63	
		Monterey			
DJF	–	–	–	–	–
MAM	20	25	4	37	14
JJA	22	16	5	53	4
SON	23	13	6	54	4

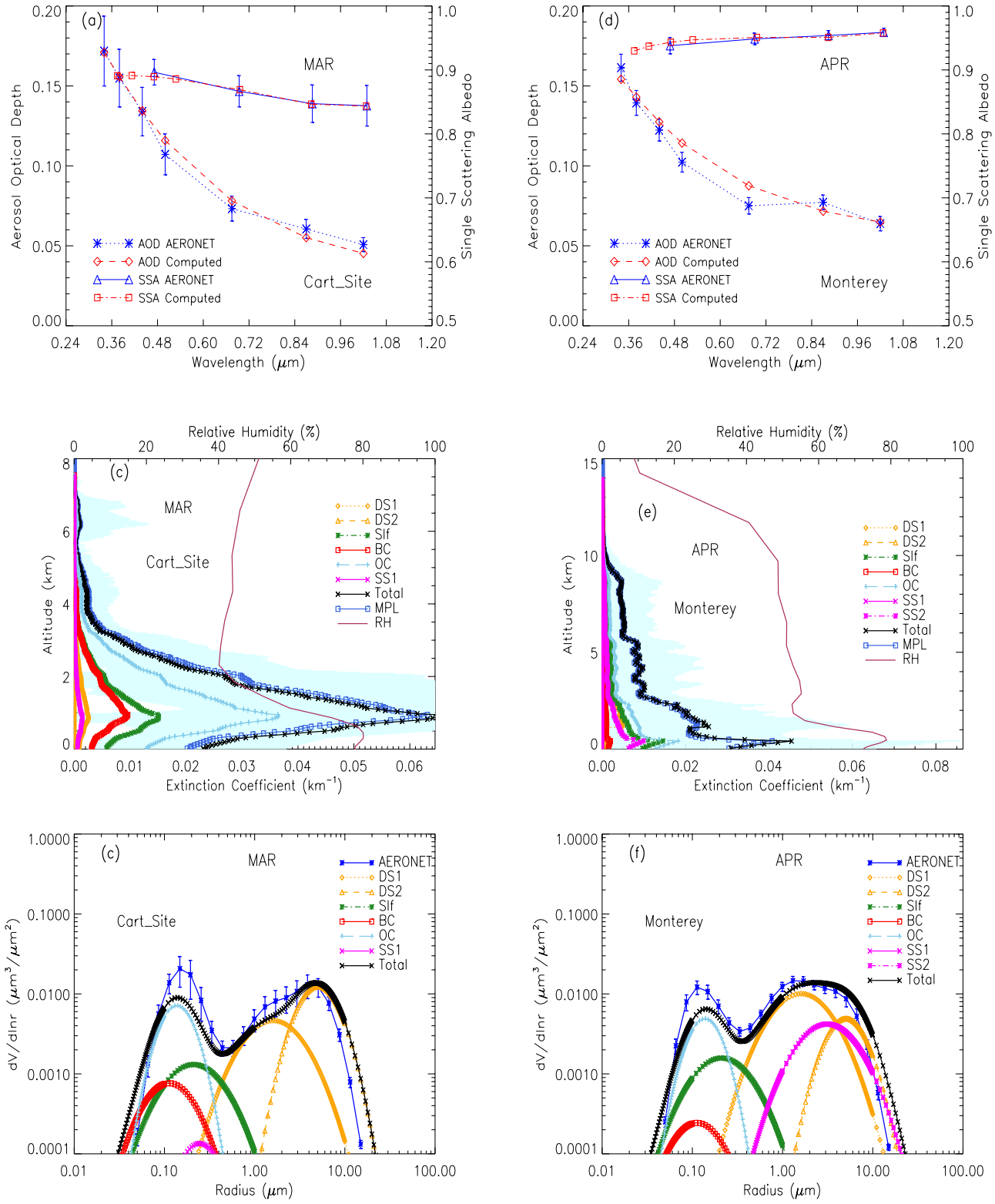

Figure 3. Comparison between observed data and computed values of major aerosol parameters based on the results of minimization for the months of (a–c) March 2002 from Cart Site and (d–f) April 2003 from Monterey. Vertical and horizontal lines in different panels have the same meaning as Figure 2.

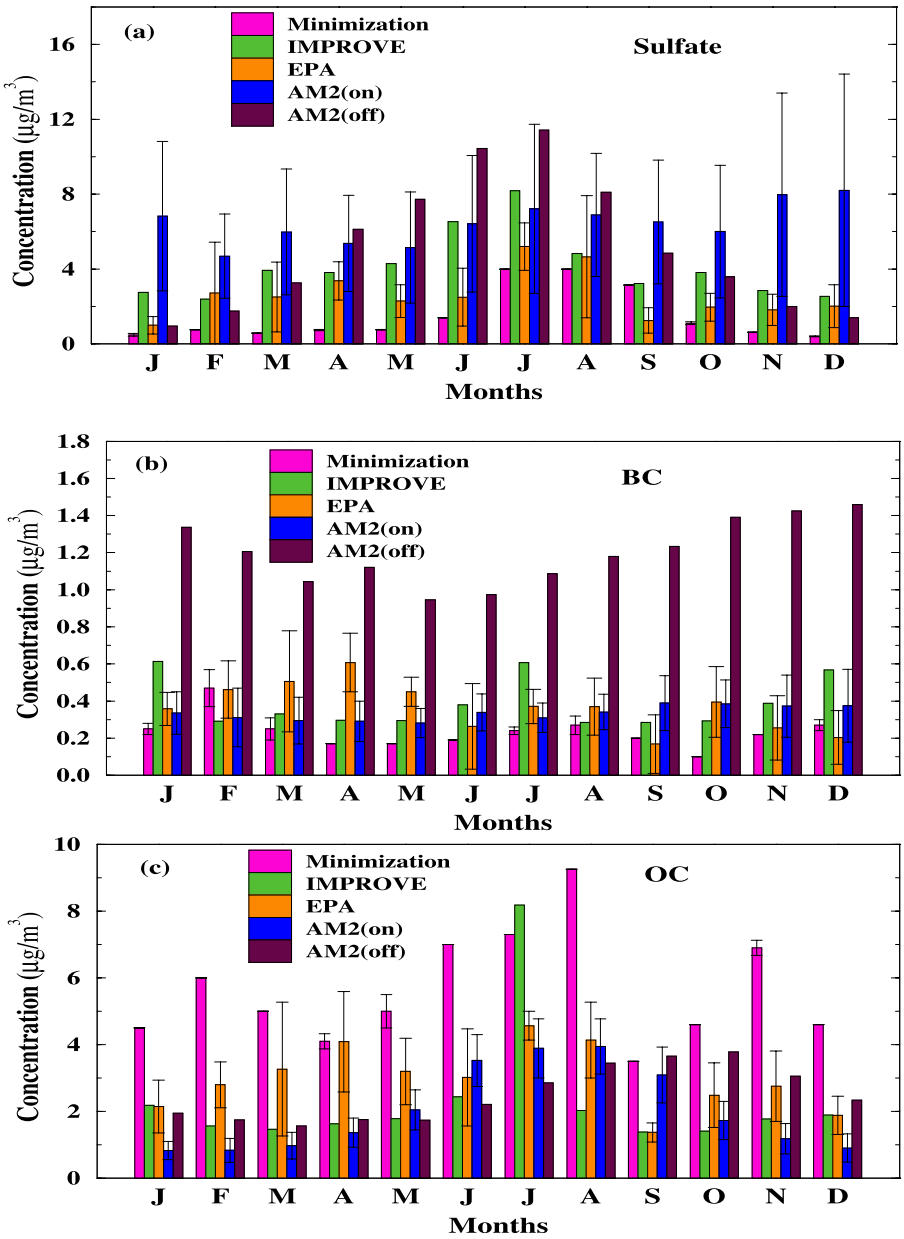

Figure 4. Comparison of surface concentration for the three aerosol species over GSFC site as retrieved by the minimization method with the monthly mean values available from IMPROVE and EPA data sets, as well as those simulated by the online and offline versions of GFDL atmospheric general circulation model (AM2).

March 2002 from Cart Site (plots a–c) and April 2003 from Monterey (plots d–f). Out of the three sites, AOD values are usually higher over GSFC, followed by Cart Site and lowest over Monterey. In general, AOD values over all sites are higher during summer months (JJA). Over Cart Site, highest values of AOD are observed in the month of August. For the selected period, relatively high values of AOD are observed at Monterey in May and June.

[35] In Figure 4a, lower values (less than 0.9 at all four wavelengths) of single scattering albedo over Cart Site during March 2002 indicates the dominance of absorbing aerosols like BC or dust in the atmosphere. Wavelength dependency of single scattering albedo with lower values in the near infrared range compared to visible wavelengths indicates the dominance of BC aerosol at Cart Site. On the other hand, single scattering albedo over Monterey site increases with λ. Dominance of non absorbing sea salt aerosols over this site results in higher values of single scattering albedo in the near infrared range while the presence of high dust loading lowers the corresponding values in the ultraviolet region.

6.2.2. Extinction Profiles

[36] Figures 3b and 3e show the monthly mean extinction profiles from the Cart Site and Monterey for the months of March 2002 and April 2003 respectively. These plots also show the extinction profiles of individual aerosol components and the total extinction due to all components based on our minimization. The maroon line in both these plots

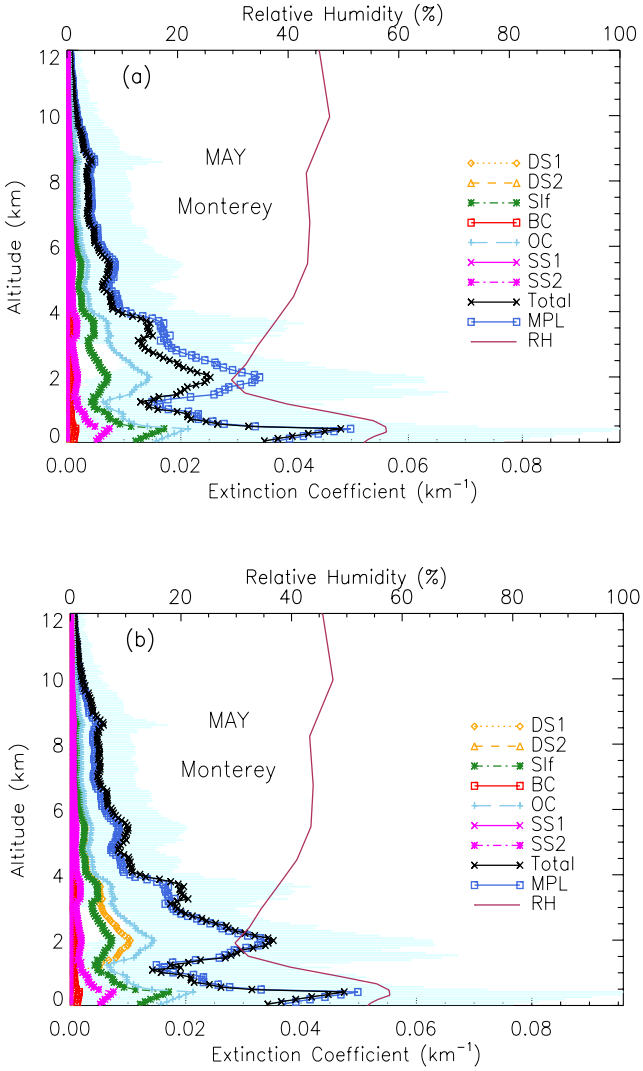

Figure 5. Comparison of vertical profile of aerosol components for two cases, (a) with no elevated layer considered and (b) with an elevated aerosol layer above 1.2 km. It can be seen that the differences between observed profile (marked as MPL) and the one corresponding to the sum of all aerosol components (marked as Total) are minimum when such an elevated aerosol layer is included. Horizontal lines in both panels have the same meaning as Figure 2.

represents the monthly mean profile of relative humidity over the respective locations obtained from NCEP reanalysis data. The profile shown for March is an example of the typical pattern of aerosol extinction profiles observed over Cart Site during different months. The pattern looks similar to the extinction profile observed over GSFC during July 2002 (Figure 2). Extinction profiles over Cart Site are characterized by a peak at higher altitude, usually between 0.5 and 1.5 km above the surface. Here we find that extinction coefficients first increase with height to reach a maxima with values which are two to three times higher than at the surface, and thereafter decrease with height to become almost nil between 4 and 6 km, depending on the season. As discussed in the case of GSFC, relative humidity plays an important role in modulating the extinction coefficient of aerosols over Cart Site, particularly in the lowest 1 km of the atmosphere.

[37] Out of the three sites, Monterey appears to be special because the extinction profiles over this location are often characterized by the presence of elevated aerosol layers (up to 9 km) in the atmosphere. This is mainly observed during spring and summer time [*Jaffe et al.*, 1999]. It is very unusual to find locally produced aerosols lifted to such high levels in the absence of very strong convection in the troposphere or any volcanic eruption. In presence of such elevated aerosol layers, our original algorithm could fail to provide a solution within acceptable uncertainty. Such a situation requires expanding the number of components in the minimization process beyond seven. However, the restriction that applies here is that the total number of components in the minimization process should not exceed 13 (which is the total number of known parameters used for comparison), otherwise the problem becomes ill constrained. We carried out all our retrievals for this site using a slightly modified algorithm, which takes into account such elevated aerosol layers. For this, we first identified the base of the elevated layer. For example, as shown in Figure 3e, the elevated layer during April starts from 1.2 km above surface. We assume here that all aerosol layers are well mixed within it and our assumption in the form of equation (4) remains valid inside each layer. Subsequently, we carried out the minimization process using 12 (7 + 5) components where five of them are distributed only above 1.2 km. We did not consider the two coarse mode components, large dust (Ds2) and sea salt (SS2) aerosol as part of the transported plume. There is a multiplicity of aerosol components in the upper layer, e.g., sulfate in this layer could be either locally produced or a part of the transported plume. In our algorithm, we treat these two sulfates as independent components.

[38] The results of our retrieval reveal that the elevated aerosol layers over Monterey site during the months of April and May are mainly constituted by small dust (Ds1) aerosols. Our results are in agreement with the earlier studies by *Jaffe et al.* [1999] and *VanCuren and Cahill* [2002], which traced back the origin of these elevated layers to the dust sources in Asia. In order to know how the results of our minimization could have been affected if the elevated layers were not taken in to account, we carried out an additional retrieval corresponding to May 2003 data from Monterey. Figure 5 shows the comparison of vertical profile of aerosol components for two cases, (Figure 5a) with no elevated layer and (Figure 5b) with an elevated aerosol layer above 1.2 km. It can be seen from Figure 5 that the differences between observed profile and the one corresponding to the sum of all aerosol components are minimum when the elevated aerosol layer is included. We also find that when such a layer is included, results for the surface concentration of components like sulfate, BC and OC are not much effected but the dust concentrations at the surface decrease.

[39] Our results show that organics contribute in the range of 35 to 60% toward the annual mean AOD over Cart Site. The contribution of sulfate is maximum in summer (around 30%) and relatively low in winter and spring (~16%). Out of the three locations, BC has maximum contribution over Cart Site (nearly 20% during February to May). The dust

contribution to AOD is also significant (12–25%) over this location. As in other sites, organics cause maximum contribution (35–55%) to the total extinction over Monterey. The contribution of sulfate varies between 13–25% with larger share in April and May. Dust contributes nearly 20% to AOD during all months. Sea salts contribute about 14% during April–May period but its contributions are less than 5% in other months. However, our retrieval for Monterey site could be associated with higher uncertainty compared to other two sites.

6.2.3. Size Distribution

[40] Figures 3c and 3f show the volume size distribution of aerosols over Cart Site and Monterey for the months of March 2002 and April 2003 respectively. Similar to GSFC site, size distribution pattern from both these sites show the presence of two modes corresponding to fine and coarse range particles. The size distribution obtained from AERONET observations are fitted by lognormal modes of individual aerosol components with concentrations based on the results of minimization. The black curves in both these plots represents the total size distribution obtained as the sum of distributions for individual components. Size distribution patterns over both these sites are characterized by the presence of a stronger coarse mode fraction compared to observations from GSFC site. This is clearly due to higher loading of dust aerosols in the atmospheric column over both these sites. However, as discussed earlier, it is organics and sulfate aerosols which largely contribute toward the extinction coefficient and AOD over all these sites.

7. Comparison of Results With Observation and Model Output

[41] In this section we discuss the comparison of near surface concentrations of aerosol components retrieved by our technique with the ground based measurements available from IMPROVE and EPA stations. We also compare our results with the concentrations simulated by two different versions of the GFDL Atmospheric General Circulation model AM2 model at the nearest grid points with respect to the chosen sites. First version is the GFDL-AM2 model with online aerosols as described in section 3 (hereafter referred as AM2(on)) and the other one is a slightly older version of AM2 with aerosol distributions simulated offline using the MOZART-2 global chemical transport model which is described by *Horowitz et al.* [2003] and evaluated in great detail by *Ginoux et al.* [2006] (hereafter referred as AM2(off)). The purpose of comparing our results with both these versions of AM2 is to find improvements in the recent online version of the model with respect to its previous offline version and understand what continues to pose problems in AM2(on). Since IMPROVE data includes only PM2.5 aerosols and excludes sea salt aerosols in their analyses, we present our comparison for the three key aerosol species; sulfate, OC, and BC, which contribute the most toward the main optical properties of interest, namely AOD and single scattering albedo of the composite aerosols.

[42] Figure 4 shows the surface concentration of three major aerosol species obtained from various sources over the GSFC site. In Figure 4, vertical lines on top of each bar corresponding to EPA and AM2(on) represents the standard deviation ($\pm 1\sigma$) in aerosol concentration about their monthly mean values. Spread in concentration values estimated by our technique, assuming a range of uncertainties associated with the input parameters like single scattering albedo and size distribution, are also shown as vertical lines corresponding to the results of minimization. For each month, we carried out several sensitivity tests using various combinations of error estimates in single scattering albedo varying in the range of 0.01 to 0.05 and the relative error in size distribution (C_{vf} and C_{vc}) varying in the range of 20–90% (see section 8 for more detail). It can be noticed from Figure 4 that sulfate and OC concentrations from all data sets exhibit a kind of seasonal variation with higher values during summer and relatively lower values during winter. Earlier, *Kinne et al.* [2006] reported about a general underestimation in the seasonality of aerosol loading over this region by most aerosol models.

[43] No clear pattern seems to be present in the seasonal variation of BC, except those from AM2(off) show higher values in winter and relatively lower values during spring and summer months. In fact, BC concentrations from AM2(off) are almost two times more than all other data sets, clearly indicating an overestimation of BC in AM2(off). In general, sulfate concentrations from AM2(on) are the highest among all data sets. On the other hand, sulfate concentrations from AM2(off) exhibit a large seasonal variation with lower values during winter months when they are close to the results of minimization as well as those from IMPROVE and EPA. However, the sulfate concentrations from AM2(off) become comparable and even higher than AM2(on) during summer months. Results of our retrieval suggest a much lower concentration of sulfate aerosols and higher concentrations of organic aerosols as compared to those simulated by both versions of AM2 model, particularly over the North-East United States. Our results are in full agreement with the findings of *Heald et al.* [2005] which showed that organic aerosols have a much stronger role to play than what has been conventionally ascribed to it in most aerosol transport models and GCMs.

[44] Table 5 lists the surface concentration of major aerosol components viz. sulfate, BC and OC over all the three sites as inferred using the current minimization technique, data available from the IMPROVE and the EPA network and those simulated by the two different versions of the GFDL-AM2 model. All concentrations are averaged in groups of three months to compare the seasonal variation of these aerosol components. In Table 5, uncertainties assigned with the results of minimization are estimated on the basis of a range of sensitivity tests carried out with respect to the error values associated with various parameters used in the minimization process as discussed in section 8. A common feature observed in the results of minimization from all sites is that the ratio of sulfate to BC mass is about ten times higher during summer months (JJA) compared to winter (DJF) and spring (MAM) months. Among all aerosol components, we see a relatively better match for BC concentrations as retrieved by our minimization method and the values available from IMPROVE and EPA measurements, particularly over GSFC and Cart site. Usually, BC concentrations from AM2(on) are slightly higher than the results of minimization but show a more or less good agreement with EPA values within $\pm 1\sigma$

Table 5. Surface Concentration of Major Aerosol Components Over the Three AERONET Sites Derived Using the Minimization Method, Measurement Data Available From IMPROVE and EPA Network, and the Values Simulated by the Offline and Online Versions of GFDL-AM2 Model

	GSFC														
	Sulfate					Black Carbon					Organic Carbon				
Months	Minz.	IMP	EPA	AM2(on)	AM2(off)	Minz.	IMP	EPA	AM2(on)	AM2(off)	Minz.	IMP	EPA	AM2(on)	AM2(off)
							GSFC								
DJF	0.54 ± 0.21	2.36	1.92	9.15	1.37	0.38 ± 0.12	0.41	0.34	0.53	1.33	4.6 ± 0.72	1.95	2.28	1.02	2.01
MAM	0.69 ± 0.13	4.35	2.72	8.64	5.70	0.21 ± 0.06	0.37	0.52	0.50	1.04	4.7 ± 0.44	1.61	3.52	1.32	1.69
JJA	3.13 ± 1.23	8.45	4.12	10.72	9.99	0.23 ± 0.04	0.53	0.34	0.66	1.08	7.25 ± 1.08	3.10	3.91	2.46	2.83
SON	1.63 ± 1.22	3.96	1.68	9.72	3.47	0.17 ± 0.05	0.41	0.27	0.64	1.35	4.80 ± 1.54	1.71	2.21	1.77	3.50
							Cart Site								
DJF	0.44 ± 0.04	1.41	1.87	4.05	0.83	0.57 ± 0.05	0.28	0.40	0.28	0.53	2.70 ± 0.16	1.21	2.98	0.38	1.05
MAM	0.21 ± 0.10	2.95	3.31	5.90	3.07	0.23 ± 0.11	0.36	0.41	0.30	0.46	2.08 ± 0.85	1.48	3.27	1.18	1.01
JJA	3.73 ± 1.69	3.41	3.84	7.55	6.84	0.26 ± 0.15	0.32	0.33	0.30	0.54	9.75 ± 1.86	2.14	4.61	1.68	1.63
SON	2.40 ± 0.42	1.81	2.25	6.38	3.16	0.18 ± 0.04	0.27	0.30	0.33	3.16	11.20 ± 1.08	1.38	3.23	0.75	2.19
							Monterey								
DJF	–	0.48	1.10	0.94	0.80	–	0.22	1.69	0.35	0.43	–	1.15	8.68	1.13	0.68
MAM	0.88 ± 0.37	0.93	1.06	0.80	1.15	0.10 ± 0.02	0.14	0.56	0.25	0.35	3.00 ± 1.03	1.18	4.02	1.03	0.67
JJA	0.93 ± 0.69	1.31	1.74	1.16	1.35	0.08 ± 0.02	0.26	0.50	0.31	0.59	3.05 ± 1.54	1.82	4.5	2.02	2.36
SON	0.59 ± 0.34	1.06	1.68	0.85	1.12	0.07 ± 0.03	0.47	1.16	0.34	0.63	2.53 ± 1.60	1.66	7.33	1.62	2.14

variation. However, during some seasons, BC values from EPA measurements over Monterey show very high values compared to all other data. Usually OC values from our retrievals are closer to EPA measurements over all sites, although there are exceptions during certain months. However, OC values from IMPROVE are usually low compared to our results of minimization for all sites. It is worth mentioning here that in general the OC concentrations from IMPROVE are also lower than the measurements reported by *Zhang et al.* [2007].

[45] It is evident from Figure 4 and Table 5 that in spite of obtaining a reasonably good match between the observed and computed values of aerosol parameters over all three locations, there are discrepancies between the results of minimization and measurements available from IMPROVE and EPA sites. We also notice differences between our results and concentrations simulated by both versions of the GFDL-AM2 model. There could be multiple reasons for these differences in aerosol concentrations from different sources. One is the inherent differences in temporal and spatial scales of averaging associated with different data sources. Comparisons presented in Figure 4 and Table 5 are made for monthly mean values of aerosol concentration whereas there are some differences in observation time and averaging procedure adopted by different data sources. Our retrievals are primarily based on AERONET observations conducted exclusively during daytime and under clear sky conditions which are usually limited during most months over the chosen sites. Aerosol sampling for the IMPROVE and EPA networks occurs irrespective of sky conditions. Under the IMPROVE program, 24-hour samples are collected twice weekly, while EPA sites collect 24-hours aerosol samples once or twice a week; not necessarily the same days as the IMPROVE network. Since IMPROVE sites are located in Class 1 Visibility protected areas, such as National Parks, Monuments, and Wilderness Areas in the United States which are not as close to the AERONET/MPL sites of interest as the EPA stations, we interpolated all data available from the IMPROVE sites onto a 1 × 1 grid map over the entire United States, and then used the nearest grid point for further comparison [*Ginoux et al.*, 2006]. The interpolation weights data inversely with the square of its distance from the grid point. In the case of EPA data, we have directly used data available from the closest station with respect to the AERONET site. This may explain some of the differences between IMPROVE and EPA data from similar locations.

[46] Differences between the results of minimization and measurements available from the IMPROVE and the EPA sites could also mean that some of the assumptions made in our technique like using a constant lidar ratio for all vertical levels might not be valid under some situations. Besides this, there could also be issues relating to the choice of fixed size distribution parameters, optical properties and hygroscopic growth factors of individual aerosol components used for Mie computation in our study. Although we have used the widely accepted and recently reported values of these parameters from the literature (see section 3), it still involves a lot of assumptions which require more verification and further validation.

8. Sensitivity Study

[47] As discussed earlier, the present method requires several observational parameters for the retrieval of aerosol concentrations over specific locations. In this section, we discuss the results of some sensitivity tests carried out to assess the effect of uncertainties associated with these parameters on the retrieval accuracy of aerosol concentrations using this technique. For this purpose, we varied the error estimate of any one parameter at a time while used the same error values for all other parameters and repeated the minimization process to find out changes in aerosol concentrations retrieved by the technique. Since the errors associated with single scattering albedo from AERONET sites are dependent on total aerosol loading in the atmosphere, we repeated all these sensitivity tests for a high AOD ($\geq$0.5 at 0.44 μm) and a low AOD case. Available data from GSFC site corresponding to the months

Table 6. Results of Minimization From Various Sensitivity Tests Carried out Using Different Error Estimates of Single Scattering Albedo and Size Distribution of Aerosols Under Low (January) and High (July) AOD Conditions Over the GSFC Site

Error in		January							July						
		Ds1	Ds2	Slf	SS1	SS2	BC	OC	Ds1	Ds2	Slf	SS1	SS2	BC	OC
SSA	C_{vf} & C_{vc} (%)	(μg/m^3)							(μg/m^3)						
0.01	60	5.25	8.5	0.33	0.01	0.04	0.25	4.5	4.3	4.3	3.7	0.05	0.11	0.20	7.3
0.02	60	4.75	8.5	0.33	0.01	0.04	0.25	4.5	3.7	4.3	3.7	0.06	0.11	0.20	7.3
0.03	60	4.75	8.5	0.33	0.01	0.04	0.25	4.5	4.0	4.3	3.7	0.04	0.11	0.24	7.3
0.04	60	4.75	8.5	0.33	0.01	0.04	0.25	4.5	4.0	4.3	3.7	0.03	0.11	0.28	7.3
0.05	60	4.75	8.5	0.33	0.01	0.04	0.25	4.5	4.0	4.3	3.7	0.03	0.11	0.28	7.3
0.03	20	5.75	8.5	0.78	0.01	0.04	0.25	4.5	4.6	4.3	4.0	0.03	0.11	0.20	7.3
0.03	30	5.75	8.5	0.48	0.01	0.04	0.25	4.5	4.6	4.3	3.7	0.04	0.11	0.28	7.3
0.03	45	5.75	8.5	0.33	0.01	0.04	0.25	4.5	4.6	4.3	3.7	0.04	0.11	0.24	7.3
0.03	75	3.75	8.5	0.33	0.01	0.04	0.25	4.5	3.4	4.3	3.7	0.05	0.11	0.24	7.3
0.03	90	3.75	8.5	0.33	0.01	0.04	0.25	4.5	3.4	4.3	3.7	0.05	0.11	0.24	7.3
0.01	20	5.75	8.5	0.63	0.01	0.04	0.30	4.5	3.4	4.3	3.7	0.04	0.11	0.28	7.3
0.05	20	5.75	8.5	0.78	0.01	0.04	0.25	4.5	4.6	4.3	4.0	0.03	0.11	0.20	7.3
0.01	90	4.75	8.5	0.33	0.01	0.04	0.25	4.5	3.4	4.3	3.7	0.06	0.11	0.20	7.3
0.05	90	3.75	8.5	0.33	0.01	0.04	0.25	4.5	3.4	4.3	3.7	0.04	0.11	0.28	7.3

of January and July are used for low and high AOD cases respectively. Table 6 lists the concentrations of all seven aerosol components obtained as results of minimization from various sensitivity tests performed with absolute errors in single scattering albedo varying from 0.01 to 0.05, relative errors in C_{vf} and C_{vc} varying in the range of 20–90% while keeping the uncertainties associated with AOD to be always fixed at ±0.01 for $\lambda \geq 0.44$ μm and ±0.02 for $\lambda < 0.44$ μm. We have not performed any sensitivity study relating to AOD as the errors associated with this parameter are relatively low compared to other parameters used in the technique [*Holben et al.*, 1998; *Dubovik et al.*, 2000].

[48] In the first set of sensitivity tests we fixed the relative error in size distribution at 60% (assuming this to be the standard error in C_{vf} and C_{vc} over all stations and during all months) while increased the error in single scattering albedo from 0.01 to 0.05 and applied the minimization method on January and July data. Results from these tests show that the concentrations of most aerosol components retrieved by our technique are least affected by the errors in single scattering albedo in the above range when errors associated with other parameters are fixed at their standard values. In the low AOD case, we find only the concentration of small dust (Ds1) decreases marginally as the errors in single scattering albedo increase from 0.01 to 0.05. However in the high AOD case, we also notice BC concentrations to increase marginally with the error in single scattering albedo.

[49] Next we performed another set of sensitivity tests using the January and July data from GSFC site in which the relative errors associated with size distribution are varied in the range of 20–90% while fixed error values are used for single scattering albedo and AOD in the minimization process. Once again, in these set of tests, we find only marginal changes in the concentrations of some aerosol components but the changes are slightly different for high and low AOD cases. Our results show that as the errors associated with size distribution (C_{vf} and C_{vc}) increase in the above range while the errors for all other parameters remain fixed at their standard value, concentrations of small dust (Ds1) and sulfate aerosols retrieved using the minimization method decrease by small amount. This decrease is found to be larger for the low AOD case than in the high AOD situation. Additionally, we find a slight increase in the concentration of BC aerosols as the errors in size distribution increase under high AOD conditions. Concentration of other aerosol components remain almost unchanged in all these tests.

[50] We performed some more sensitivity tests to see the effect on the results of minimization under various possible situations when the errors in size distribution and single scattering are either very low or very high while errors in AOD are fixed at their standard value. When the errors in size distribution were fixed at 20% and the errors in single scattering albedo increased from 0.01 to 0.05, results of minimization showed a marginal increase in sulfate concentration and a simultaneous decrease in BC values under both low and high AOD conditions. Additionally, under same situations, our results also show a small increase in the small dust concentrations in the high AOD case. On the other hand, when the errors in size distribution were fixed at a high value of 90% and the errors in single scattering albedo varied in the range of 0.01 to 0.05, we notice minimal changes in the concentrations of most aerosol components except a marginal decrease in small dust concentration under low AOD conditions and a small increase BC concentration under high AOD conditions.

[51] Overall, from all these sensitivity tests listed in Table 6, we conclude that the concentration of OC, large dust (Ds2) and to some extent sea salt aerosols retrieved by our minimization technique are not affected by the errors associated with the data corresponding to single scattering albedo and size distribution of aerosols within specified limits. However, there could be errors associated with small dust (Ds1), sulfate and BC concentrations retrieved by this technique depending on the error values associated with single scattering albedo and size distribution of aerosols as well as the total aerosol loading in the atmosphere.

[52] We now discuss the results of some additional sensitivity tests on single scattering albedo, size parameter and vertical distribution of aerosols in the following subsections.

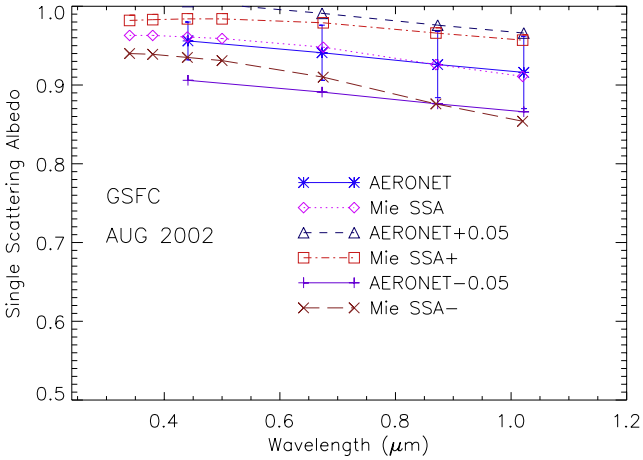

Figure 6. Comparison of reference and the estimated values of single scattering albedo for three different cases of a sensitivity study. First one is carried out using the same values of single scattering albedo as available from AERONET, whereas in other two, the AERONET values are either increased or decreased by 0.05 at all wavelengths while using the same values for all other parameters. Estimated values of single scattering albedo for the three cases described above are referred as "Mie SSA," "Mie SSA+," and "Mie SSA−," respectively.

8.1. Single Scattering Albedo

[53] Considering an absolute error of 0.05 in single scattering albedo at all four wavelengths, we performed additional sensitivity tests in which once we increased the $\omega(\lambda)$ values from AERONET by 0.05 and then decreased them all by 0.05 but used the same values for all other parameters like AOD, size distribution, extinction profiles, relative humidity etc. and repeated the minimization process. Again, we repeated both these sensitivity tests for a high AOD ($\geq$0.5 at 0.44 μm) and a low AOD case, using the available data from GSFC site for the months of August and January respectively. In all these sensitivity tests, we used the fixed standard error variances for all parameters as mentioned in section 5.4. Figure 6 shows a comparison of single scattering albedo from GSFC site and their estimated values based on three different cases of minimization tests. The first one is carried out using the same values of single scattering albedo as available from AERONET whereas in other two cases AERONET values are either increased or decreased by 0.05 while same values are used for all other parameters. Estimates of single scattering albedo based on the results of minimization for these three cases are referred as "Mie SSA," "Mie SSA+" and "Mie SSA−."

[54] We find that the estimated values of single scattering albedo shows best match with the input data when AERONET values are directly used for minimization. Our analysis shows if the offset in single scattering albedo values are large ($\sim$0.05) while those corresponding to AOD and size distribution are small, it is often difficult to find any combination of aerosol concentration which simultaneously minimizes the differences between observed and computed values of all parameters. Table 7 presents a comparison of surface concentration of aerosols retrieved in the above sensitivity tests. Here concentrations corresponding to *SSA*, *SSA+* and *SSA−* refers to the results of minimization obtained using the same values of single scattering albedo as obtained from AERONET, increasing their values by 0.05 and decreasing them all by 0.05 respectively. We find the results of minimization to be more sensitive to the offset in single scattering albedo under high AOD conditions.

[55] Out of all aerosol components, the retrieval of BC appears to be most sensitivity to the accuracy of single scattering albedo. Results show that under high AOD conditions, errors in the retrieval of BC could be as high as 100% when there is a large bias of $\sim$0.05 in the reference value of single scattering albedo. We find sulfate concentrations to either increase or exhibit no change in the *SSA+* case while their values decrease in the *SSA−* case with respect to *SSA* case. Thus errors in the retrieval of sulfate concentration are large when there is a negative bias in single scattering albedo values under both low AOD and high AOD conditions. Retrieval of organics is found to be the least sensitive to the offset in single scattering albedo, particularly during low AOD conditions.

8.2. Size Parameter

[56] As discussed earlier (in section 7), the uncertainties associated with the choice of fixed size distribution parameters of individual aerosol components as given in Table 1 could also contribute to the overall uncertainty in the retrieval of aerosol concentration using this technique. Although we used the widely accepted and recently reported values of all these parameters from the literature, there are some uncertainties associated with each of them. In order to get an idea about the sensitivity of our results with respect to

Table 7. Surface Concentration (μg/m^3) of Aerosol Components Corresponding to Different Sensitivity Tests on Single Scattering Albedo[a]

	High AOD Case			Low AOD Case		
Component	SSA	SSA+	SSA−	SSA	SSA+	SSA−
Sulfate (Slf)	4.0	4.2	2.5	0.48	0.48	0.32
Black carbon (BC)	0.27	0.01	0.51	0.3	0.15	0.42
Organic carbon (OC)	8.75	8.6	11.0	4.0	4.0	3.9
Dust small (Ds1)	2.6	2.8	5.0	5.75	5.8	6.6
Dust large (Ds2)	5.0	5.5	6.0	8.5	8.0	8.5
Sea salt small (SS1)	0.03	0.08	0.03	0.01	0.05	0.01
Sea salt large (SS2)	0.08	0.18	0.02	0.12	0.17	0.05

[a]Here concentrations corresponding to *SSA*, *SSA+* and *SSA−* refers to the results of minimization obtained using the same values of single scattering albedo as available from AERONET, increasing them by 0.05 and decreasing them all by 0.05 respectively.

Table 8. Surface Concentration ($\mu g/m^3$) of Aerosol Components Retrieved by the Minimization Method Corresponding to Different Sensitivity Tests on the Size Parameters of Sulfate Aerosol

σ	r_{modN}	Ds1	Ds2	Slf	SS1	SS2	BC	OC
(μm)		($\mu g/m^3$)						
2.0	0.05	4.0	4.3	3.7	0.04	0.11	0.24	7.3
2.0	0.045	4.9	4.9	3.45	0.06	0.09	0.16	7.9
1.9	0.05	4.6	4.9	4.9	0.02	0.06	0.18	4.3
2.1	0.05	3.4	5.1	3.6	0.02	0.03	0.23	8.4

the uncertainties involved with these parameters, we performed some additional sensitivity tests in which we purposely changed the size parameters of one aerosol component marginally and repeated the minimization process. As an example, we performed these sensitivity tests with respect to the size parameters of sulfate aerosol. Table 8 lists the surface concentration of all aerosol components as retrieved by the minimization method for different choices of size parameters of sulfate aerosol while using the same parameters for all other components as listed in Table 1. The results of our sensitivity study show that the errors in the estimated values of aerosol concentration could be up to 50% due to the uncertainties associated with the choice of size parameters of individual aerosol components. This error estimate is smaller than other uncertainties associated with our retrievals due to possible biases in the reference values of single scattering albedo obtained from AERONET products.

8.3. Vertical Distribution

[57] An important parameter used in our minimization method is the vertical profile of aerosols. In order to understand the sensitivity of our results to the vertical distribution of aerosols, we repeated the retrieval for July 2002 over the GSFC site using three arbitrary vertical distributions in addition to the actual distribution (VD0) obtained from MPLNET. In the first case (VD1), we assume all aerosols to be uniformly mixed in a 2.5 km thick layer above the surface. In the next two distributions named VD2 and VD3, we consider a well mixed layer of thickness 2 km and 0.5 km respectively at the bottom, above which all concentrations decrease exponentially with a scale height of 1 up to 5 km from the surface. Table 9 lists the surface and total column concentration of aerosol components retrieved using the above choices of vertical distribution. Results of these sensitivity tests show that the retrieved concentration at the surface (or any particular level) is largely dependent on the choice of the vertical distribution of aerosols. However, the column burden seems to be less sensitive to these changes. The noted differences in column burden are mainly caused by the differences in hygroscopic growth experienced by the aerosols under different vertical distributions. If all aerosols were nonhygroscopic or the relative humidity remained constant with altitude, retrievals for the column burden aerosols would be independent of their vertical distribution. In the above tests, column burden of nonhygroscopic components also change by small amounts because they try to compensate for the changes in hygroscopic components and optimize the composite AOD, single scattering albedo and size distribution of aerosols in the minimization process. Thus the knowledge on vertical distribution of aerosols is crucial for an accurate retrieval of concentrations at any particular level, although it may be possible to retrieve the column burden of aerosols within the uncertainties of our technique using any arbitrary distribution.

9. Discussion

[58] First major advantage of our technique over similar studies carried out earlier using only AERONET data is the ability to separate the contributions of all major aerosol components like sulfate, OC, BC, dust and sea salt to the total aerosol loading. Secondly, the inclusion of vertical profile from MPLNET makes it possible to retrieve not just the column burden of aerosols but also their concentration at the surface. This in turn allows us to do a direct comparison of our retrievals with the available measurements, which are mostly ground based, and also in the validation of GCM output. Earlier, *Schuster et al.* [2005] used a different methodology and a different set of assumptions such as the Maxwell Garnett effective medium approximation for a three component internal mixture of water, ammonium sulfate and BC to infer the BC column burden using the AERONET data over "low dust" regions. Comparison of our results with *Schuster et al.* [2005] show that the column burden of BC estimated by *Schuster et al.* [2005] over the North American sites are ~2.5 times higher than our retrievals. However, in difference with our approach, *Schuster et al.* [2005] did not account for the absorbing properties of OC and dust aerosol and attributed all aerosol absorption to BC. This could likely lead to an overestimation of BC amount in the approach of *Schuster et al.* [2005] and, at least in part, explain the differences with our results. Our result suggests higher concentration of OC and lower concentration of sulfate aerosols over the North-East United States than what is simulated by both versions of AM2 model, which is in agreement with the findings of *Heald et al.* [2005].

Table 9. Surface (Srf. in $\mu g/m^3$) and Total Column (Col. in mg/m^2) Concentration of Major Aerosol Components Retrieved by the Minimization Method for July 2002 Over GSFC Using Different Vertical Distribution of Aerosol Described in Section 8.3

	Ds1		Ds2		Slf		SS1		SS2		BC		OC	
Profile type	Surf.	Col.	Surf.	Col.	Surf.	Col.	Surf.	Col.	Surf.	Col.	Surf.	Col.	Surf.	Col.
VD0	4.0	23	4.3	24	3.7	45	0.04	0.9	0.11	2.6	0.23	1.3	7.	52
VD1	9.0	22	10	25	11.5	48	0.15	1.1	0.65	4.6	0.69	1.7	15.8	41
VD2	9.0	26	9.5	27	10	48	0.1	0.8	0.45	3.6	0.6	1.7	14.5	44
VD3	16	23	17	24	18.5	46	0.18	0.7	0.8	3.4	1.1	1.6	26.5	40

[59] Our present study is based on the assumption of external mixing of aerosols. In principle, there can be both external and internal mixing of aerosols. However, the aerosol mixing state is not completely clear at this moment. There are studies that suggest the internal mixing [*Schuster et al.*, 2005] while some other identify the external mixing as most probable mechanism [*Mallet et al.*, 2004]. More analysis of this issue is needed, however as this work is an initial attempt of its kind, we adopt the simplest and the most transparent approach. More complex approaches such as a combination of external and internal mixing of aerosols will be undertaken in future efforts. We understand that our technique has limitations, however, this simple method when used with CALIOP and AERONET observations can become a useful tool for the modelers to evaluate their model results, within the uncertainties of our retrieval, over regions where otherwise no data on aerosol composition is available.

10. Summary and Conclusions

[60] For a realistic and meaningful assessment of the impacts of aerosols on climate, it is crucial to evaluate model results globally by comparing them with observations. Only satellite instruments provide a global coverage but only for limited aerosol parameters such as AOD. Comparison of AOD may not be sufficient to understand and resolve discrepancies between model results and observations because AOD is not necessarily the prognostic variable in global aerosol models, which actually predicts quantities like aerosol mass and number concentration. There has been several attempts to relate satellite derived AOD with near surface PM2.5 concentration [*Liu et al.*, 2004, 2005; *Al-Saadi et al.*, 2005]. These studies are primarily based on some empirical relation derived from the regression analysis between the measurements of surface PM2.5 concentration and satellite derived AOD values. However, most of these studies ignored the vertical profile of aerosols and more recently *Wang and Martin* [2007] and *Shinozuka et al.* [2007] emphasized on proper treatment of aerosol hygroscopicity and mixing state in satellite retrieval of AOD and its correlation with the estimation of PM2.5 concentration.

[61] In this paper, we present a method to derive the concentration of aerosol components from the measurements of multiple aerosol parameters such as spectral values of AOD and single scattering albedo along with their size distribution and extinction profile. The main objective of this work is to offer a technique that provides aerosol concentrations derived from optical measurements in places where no direct measurements of aerosol composition are available. This could be useful to validate model results and in future derive additional information from satellite retrievals. The technique involves finding the best combination of aerosol concentration by minimizing the difference between the measured and the calculated spectral variation of optical properties (AOD and single scattering albedo) and size distribution. The method has been applied to retrieve the seasonal variation of aerosol composition over three sites located in three different regions of the United States (West coast, Great Plains, and North East), using AERONET and MPLNET data. Our technique makes use of direct and retrieved AERONET data such as optical depth at seven wavelengths, single scattering albedo at four wavelengths and volume fraction of the coarse and fine mode aerosol size distribution. The MPLNET lidar data provides a vertical constraint on the derived profile of extinction coefficient for the entire troposphere. The results of our technique are then compared with the measured concentration of aerosol components from two sources (IMPROVE and EPA) as well as the newly developed aerosol module in the GFDL climate model (AM2). In general, concentrations of major aerosol components retrieved by our technique compare well with the ground-based measurements available from the three sites. However, there are some discrepancies in the monthly mean comparison due to the inherent differences in temporal and spatial scales of averaging associated with different data sources or some of the assumptions made in our study. Comparison of results show that over continental North America, the online version of AM2 overestimates sulfate concentration approximately by a factor of two and underestimates organic carbon by nearly the same amount. On the other hand, the offline version of AM2 overestimates BC concentration by at least a factor of two with respect to the results of minimization as well as other measurement data available over the region during all seasons. In this case, the online version of the model shows an improvement and better compares with the observations as well the results of our minimization. Sulfate concentrations from the offline version of AM2 compare well with our results and other measurement data during winter months. Results of our sensitivity study show that the errors in the retrieval of black carbon and sulfate concentrations could be as high as 100% when there is a large bias of $\sim$0.05 in the reference values of single scattering albedo under high AOD ($\geq$0.5 at 0.44 μm) conditions. Retrieval of organics seems to be less sensitive to the errors in single scattering albedo as well as size distribution, particularly under low AOD conditions. Knowledge on vertical distribution is crucial for an accurate retrieval of surface concentration of aerosols. We also show that it is possible to detect the composition and concentration of elevated aerosol layers using our technique.

[62] So far, the technique has been applied over the United States where the results could be evaluated by comparing with ground-based measurements of aerosol composition, but our objective is to apply it at places where such measurements are not available. Unfortunately there are only a few places with collocated Sun photometer and lidar instruments outside the US. Since July 2006, the lidar instrument CALIOP (Cloud-Aerosol LIdar with Orthogonal Polarization) on board the CALIPSO (The Cloud-Aerosol Lidar and Infrared Pathfinder Satellite Observation) platform has been sweeping the Earth measuring vertical profile of normalized backscattering coefficient. This data has been largely used for cloud properties but some studies on aerosol properties have been recently published [*Uno et al.*, 2008]. Our future intention is to improve the current minimization technique by incorporating CALIOP data along with AERONET observations and thereby retrieve the aerosol composition over Asia. Eventually this technique could also be applied for the retrieval of air quality by calculating PM2.5 and PM10 concentrations. This might improve the existing method developed by *Chu et al.* [2003]

by providing a better relation between surface measurements of PM2.5 concentration and satellite data. We understand that our technique has limitations, however, this simple but robust method when used with CALIOP and AERONET observations can become a useful tool for the modelers to evaluate their model results, within the uncertainties of our retrieval, over regions where otherwise no data on aerosol composition is available.

[63] **Acknowledgment.** The Lidar data from Cart Site were obtained from the archive of the Atmospheric Radiation Measurement Climate Research Facility which is supported by the Department of Energy, United States of America.

References

Ackerman, A. S., O. B. Toon, D. E. Stevens, A. J. Heymsfield, V. Ramanathan, and E. J. Welton (2000), Reduction of tropical cloudiness by soot, *Science*, *288*, 1042–1047.

Al-Saadi, J., et al. (2005), Improving national air quality forecasts with satellite aerosol observations, *Bull. Am. Meteorol. Soc.*, *86*, 1249–1261.

Balkanski, Y. J., D. J. Jacob, G. M. Gardner, W. C. Graustein, and K. K. Turekian (1993), Transport and residence times of tropospheric aerosols inferred from a global three-dimensional simulation of ^{210}Pb, *J. Geophys. Res.*, *98*, 20,573–20,586.

Balkanski, Y., M. Schulz, T. Claquin, and S. Guibert (2007), Reevaluation of Mineral aerosol radiative forcings suggests a better agreement with satellite and AERONET data, *Atmos. Chem. Phys.*, *7*, 81–95.

Bergstrom, R. W., P. B. Russell, and P. Hignett (2002), The Wavelength dependence of black carbon particles: Predictions and Results from the TARFOX experiment and Implications for the Aerosol Single Scattering Albedo, *J. Atmos. Sci.*, *59*, 567–577.

Bohren, C. F., and D. R. Hoffman (1998), *Absorption and Scattering of Light by Small Particles*, pp. 339–342, Wiley, New York.

Campbell, J. R., D. L. Hlavka, E. J. Welton, C. J. Flynn, D. D. Turner, J. D. Spinhirne, V. S. Scott, and I. H. Hwang (2002), Full-time, eye-safe cloud and aerosol lidar observation at atmospheric radiation measurement program sites: Instrument and data processing, *J. Atmos. Ocean. Technol.*, *19*, 431–442.

Chin, M., P. Ginoux, S. Kinne, O. Torres, B. N. Holben, B. N. Duncan, R. V. Martin, J. A. Logan, A. Higurashi, and T. Nakajima (2002), Tropospheric aerosol optical thickness from the GOCART model and comparisons with satellite and Sun photometer measurements, *J. Atmos. Sci.*, *59*(3), 461–483.

Chu, D. A., Y. J. Kaufman, G. Zibordi, J. D. Chern, J. Mao, C. Li, and B. N. Holben (2003), Global monitoring of air pollution over land from the Earth Observing System-Terra Moderate Resolution Imaging Spectroradiometer (MODIS), *J. Geophys. Res.*, *108*(D21), 4661, doi:10.1029/2002JD003179.

Chung, C. E., V. Ramanathan, D. Kim, and I. A. Podgorny (2005), Global anthropogenic aerosol direct forcing derived from satellite and ground-based observations, *J. Geophys. Res.*, *110*, D24207, doi:10.1029/2005JD006356.

Dentener, F., et al. (2006), Emissions of primary aerosol and precursor gases in the years 2000 and 1750, prescribed data-sets for AeroCom, *Atmos. Chem. Phys.*, *6*, 4321–4344.

Dubovik, O., and M. D. King (2000), A flexible inversion algorithm for retrieval of aerosol optical properties from Sun and sky radiance measurements, *J. Geophys. Res.*, *105*, 20,673–20,696.

Dubovik, O., A. Smirnov, B. N. Holben, M. D. King, Y. J. Kaufman, T. F. Eck, and I. Slutsker (2000), Accuracy assessments of aerosol optical properties retrieved from AERONET Sun and sky-radiance measurements, *J. Geophys. Res.*, *105*, 9791–9806.

Dubovik, O., B. N. Holben, T. F. Eck, A. Smirnov, Y. J. Kaufman, M. D. King, and I. Slutsker (2002), Variability of absorption and optical properties of key aerosol types observed in worldwide locations, *J. Atmos. Sci.*, *59*, 590–608.

Eck, T. F., B. N. Holben, J. S. Reid, O. Dubovik, A. Smirnov, N. T. O'Neill, I. Slutsker, and S. Kinne (1999), Wavelength dependence of the optical depth of biomass burning, urban, and desert dust aerosols, *J. Geophys. Res.*, *104*, 31,333–31,349.

Forster, P., et al. (2007), Changes in Atmospheric Constituents and in Radiative Forcing, in *Climate Change 2007: The Physical Science Basis. Contribution of Working Group I to the Fourth Assessment Report of the Intergovernmental Panel on Climate Change*, Cambridge Univ. Press, Cambridge, U. K.

Gassó, S., and D. A. Hegg (2003), On the retrieval of columnar aerosol mass and CCN concentration by MODIS, *J. Geophys. Res.*, *108*(D1), 4010, doi:10.1029/2002JD002382.

GFDL Global Atmospheric Model Development Team (2004), The new GFDL global atmosphere and land model AM2-LM2: Evaluation with prescribed SST simulations, *J. Clim.*, *17*, 4641–4673.

Ginoux, P., M. Chin, I. Tegen, J. M. Prospero, B. Holben, O. Dubovik, and S. Lin (2001), Sources and distributions of dust aerosols simulated with the GOCART model, *J. Geophys. Res.*, *106*, 22,055–22,074.

Ginoux, P., L. W. Horowitz, V. Ramaswamy, I. V. Geogdzhayev, B. N. Holben, G. Stenchikov, and X. Tie (2006), Evaluation of aerosol distribution and optical depth in the Geophysical Fluid Dynamics Laboratory coupled model CM2.1 for present climate, *J. Geophys. Res.*, *111*, D22210, doi:10.1029/2005JD006707.

Giorgi, F., and W. L. Chameides (1986), Rainout lifetimes of highly soluble aerosols and gases as inferred from simulations with a general circulation model, *J. Geophys. Res.*, *91*, 14,367–14,376.

Haywood, J., and O. Boucher (2000), Estimates of the direct and indirect radiative forcing due to tropospheric aerosols: A review, *Rev. Geophys.*, *38*, 513–543.

Haywood, J. M., and V. Ramaswamy (1998), Global sensitivity studies of the direct radiative forcing due to anthropogenic sulfate and black carbon aerosols, *J. Geophys. Res.*, *103*, 6043–6058.

Heald, C. L., D. J. Jacob, R. J. Park, L. M. Russell, B. J. Huebert, J. H. Seinfeld, H. Liao, and R. J. Weber (2005), A large organic aerosol source in the free troposphere missing from current models, *Geophys. Res. Lett.*, *32*, L18809, doi:10.1029/2005GL023831.

Hess, M., P. Keopke, and I. Schult (1998), Optical Properties of aerosols and clouds: The software package OPAC, *Bull. Am. Meteorol. Soc.*, *79*, 831–844.

Holben, B. N., et al. (1998), AERONET — A federated instrument network and data archive for aerosol characterization, *Remote Sens. Environ.*, *66*(1), 1–16.

Holben, B. N., et al. (2001), An emerging ground-based aerosol climatology: Aerosol optical depth from AERONET, *J. Geophys. Res.*, *106*, 12,067–12,098.

Horowitz, L. W., et al. (2003), A global simulation of tropospheric ozone and related tracers: Description and evaluation of MOZART, version 2, *J. Geophys. Res.*, *108*(D24), 4784, doi:10.1029/2002JD002853.

Jaffe, D., et al. (1999), Transport of Asian air pollution to North America, *Geophys. Res. Lett.*, *26*, 711–714.

Kaufman, Y. J., D. Tanre, and O. Boucher (2002), A satellite view of aerosols in the climate system, *Nature*, *419*, 215–223.

Kinne, S., et al. (2006), An AeroCom initial assessment optical properties in aerosol component modules of global models, *Atmos. Chem. Phys.*, *6*, 1815–1834.

Kiehl, J. T., and B. P. Briegleb (1993), The radiative roles of sulphate aerosols and greenhouse gases in climate forcing, *Science*, *260*, 311–314.

Li, F., P. Ginoux, and V. Ramaswamy (2008), Distribution, transport, and deposition of mineral dust in the Southern Ocean and Antarctica: Contribution of major sources, *J. Geophys. Res.*, *113*, D10207, doi:10.1029/2007JD009190.

Liu, Y., R. J. Park, D. J. Jacob, Q. Li, V. Kilaru, and J. A. Sarmat (2004), Mapping annual mean ground-level $PM_{2.5}$ concentrations using Multiangle Imaging Spectroradiometer aerosol optical thickness over the contiguous United States, *J. Geophys. Res.*, *109*, D22206, doi:10.1029/2004JD005025.

Liu, Y., J. A. Sarnat, V. Kilaru, D. J. Jacob, and P. Koutrakis (2005), Estimating ground-level PM2.5 in the eastern United States using satellite remote sensing, *Environ. Sci. Technol.*, *39*, 3269–3278.

Mallet, M., J. C. Roger, S. Despiau, J. P. Putaud, and O. Dubovik (2004), A study of the mixing state of black carbon in urban zone, *J. Geophys. Res.*, *109*, D04202, doi:10.1029/2003JD003940.

Malm, W. C., J. F. Sisler, D. Huffman, R. A. Eldred, and T. A. Cahill (1994), Spatial and seasonal trends in particle concentration and optical extinction in the United States, *J. Geophys. Res.*, *99*, 1347–1370.

Mattis, I., A. Ansmann, D. Muller, U. Wandinger, and D. Althausen (2004), Multiyear aerosol observations with dualwavelength Raman lidar in the framework of EARLINET, *J. Geophys. Res.*, *109*, D13203, doi:10.1029/2004JD004600.

Ming, Y., and L. M. Russell (2004), Organic aerosol effects on fog droplet spectra, *J. Geophys. Res.*, *109*, D10206, doi:10.1029/2003JD004427.

Ming, Y., V. Ramaswamy, P. A. Ginoux, and L. H. Horowitz (2005), Direct radiative forcing of anthropogenic organic aerosol, *J. Geophys. Res.*, *110*, D20208, doi:10.1029/2004JD005573.

Monahan, E. C., D. E. Spiel, and K. L. Davidson (1986), A model of marine aerosol generation via whitecaps and wave disruption, in *Oceanic Whitecaps and Their Role in Air-Sea Exchange Processes*, edited by E. C. Monahan and G. Mac Niocaill, pp. 167–174, D. Reidel, Dordrecht, Netherlands.

Moorthi, S., and M. J. Suarez (1992), Relaxed Arakawa-Schubert. A parameterization of moist convection for general circulation models, *Mon. Weather Rev.*, *120*, 978–1002.

Penner, J. E., et al. (2002), A comparison of model- and satellite-derived aerosol optical depth and reflectivity, *J. Atmos. Sci.*, *59*(3), 441–460.

Reddy, R. S., and O. Boucher (2004), A study of the global cycle of carbonaceous aerosols in the LMDZT general circulation model, *J. Geophys. Res.*, *109*, D14202, doi:10.1029/2003JD004048.

Schmid, B., et al. (2006), How well do state-of-the-art techniques measuring the vertical profile of tropospheric aerosol extinction compare?, *J. Geophys. Res.*, *111*, D05S07, doi:10.1029/2005JD005837.

Schuster, G. L., O. Dubovik, B. N. Holben, and E. E. Clothiaux (2005), Inferring black carbon content and specific absorption from Aerosol Robotic Network (AERONET) aerosol retrievals, *J. Geophys. Res.*, *110*, D10S17, doi:10.1029/2004JD004548.

Shinozuka, Y., A. D. Clarke, S. G. Howell, V. N. Kapustin, C. S. McNaughton, J. Zhou, and B. E. Anderson (2007), Aircraft profiles of aerosol microphysics and optical properties over North America: Aerosol optical depth and its association with PM2.5 and water uptake, *J. Geophys. Res.*, *112*, D12S20, doi:10.1029/2006JD007918.

Smirnov, A., B. N. Holben, T. F. Eck, O. Dubovik, and I. Slutsker (2000), Cloud screening and quality control algorithms for the AERONET data base, *Remote Sens. Environ.*, *73*, 337–349.

Solomon, P. A., et al. (2001), Evaluation of PM2.5 Chemical Speciation Samplers for Use in the EPA National PM2.5 Chemical Speciation Network EPA-454/R-01-005; NTIS PB 2001-105814, US EPA, Research Triangle Park, N. C., May 2001.

Tang, I. N., and H. R. Munkelwitz (1994), Water activities, densities, and refractive indices of aqueous sulfates and sodium nitrate droplets of atmospheric importance, *J. Geophys. Res.*, *99*, 18,801–18,808.

Tang, I. N., A. C. Tridico, and K. H. Fung (1997), Thermodynamic and optical properties of sea-salt aerosols, *J. Geophys. Res.*, *102*, 23,269–23,276.

Textor, C., et al. (2006), Analysis and quantification of the diversities of aerosol life cycles within AeroCom, *Atmos. Chem. Phys.*, *6*, 1777–1813.

Tie, X., S. Madronich, S. Walters, D. P. Edwards, P. Ginoux, N. Mahowald, R.-Y. Zhang, C. Lou, and G. Brasseur (2005), Assessment of the global impact of aerosols on tropospheric oxidants, *J. Geophys. Res.*, *110*, D03204, doi:10.1029/2004JD005359.

Uno, I., K. Yumimoto, A. Shimizu, Y. Hara, N. Sugimoto, Z. Wang, Z. Liu, and D. M. Winker (2008), 3D structure of Asian dust transport revealed by CALIPSO lidar and a 4DVAR dust model, *Geophys. Res. Lett.*, *35*, L06803, doi:10.1029/2007GL032329.

VanCuren, R., and T. Cahill (2002), Asian aerosols in North America: Frequency and concentration of fine dust, *J. Geophys. Res.*, *107*(D24), 4804, doi:10.1029/2002JD002204.

Van derWerf, G. R., J. T. Randerson, L. Giglio, G. J. Collatz, P. S. Kasibhatla, and A. F. Arellano Jr. (2006), Interannual variability in global biomass burning emissions from 1997 to 2004, *Atmos. Chem. Phys.*, *6*, 3423–3441.

Wang, J., and S. A. Christopher (2003), Intercomparison between satellite derived aerosol optical thickness and $PM_{2.5}$ mass: Implications for air quality studies, *Geophys. Res. Lett.*, *30*(21), 2095, doi:10.1029/2003GL018174.

Wang, J., and S. T. Martin (2007), Satellite characterization of urban aerosols: Importance of including hygroscopicity and mixing state in the retrieval algorithms, *J. Geophys. Res.*, *112*, D17203, doi:10.1029/2006JD008078.

Welton, E. J., and J. R. Campbell (2002), Micro-pulse lidar signals: Uncertainty analysis, *J. Atmos. Ocean. Technol.*, *19*, 2089–2094.

Welton, E. J., et al. (2000), Ground-based lidar measurements of aerosols during ACE-2: Instrument description, results, and comparisons with other ground-based and airborne measurements, *Tellus*, *52B*, 635–650.

Welton, E. J., J. R. Campbell, J. D. Spinhirne, and V. S. Scott (2001), Global monitoring of clouds and aerosols using a network of micro-pulse lidar systems, in *Lidar Remote Sensing for Industry and Environmental Monitoring*, edited by U. N. Singh, T. Itabe, and N. Sugimoto, *Proc. SPIE*, *4153*, 151–158.

Wesely, M. L. (1989), Parameterization of surface resistance to gaseous dry deposition in regional-scale numerical models, *Atmos. Environ.*, *23*, 1293–1304, doi:10.1016/0004-6981(89)90153-4.

Zhang, Q., et al. (2007), Ubiquity and dominance of oxygenated species in organic aerosols in anthropogenically-influenced Northern Hemisphere midlatitudes, *Geophys. Res. Lett.*, *34*, L13801, doi:10.1029/2007GL029979.

O. Dubovik, Laboratoire d'Optique Atmospherique, CNRS Universite de Lille, 1 Bat P5 Cite scientifique, 59655 Villeneuve d'Ascq, Cedex, France.

D. Ganguly, P. Ginoux, and V. Ramaswamy, NOAA, Geophysical Fluid Dynamics Laboratory, 201 Forrestal Road, Princeton, NJ 08540-6649, USA. (dilip.ganguly@noaa.gov)

B. N. Holben, NASA, Goddard Space Flight Center, Code 614.4, Greenbelt, MD 20771, USA.

E. A. Reid, Aerosol and Radiation Modeling Section, Marine Meteorology Division, Naval Research Laboratory, 7 Grace Hopper Avenue, Stop 2, Monterey, CA 93943-5502, USA.

J. Welton, NASA, Goddard Space Flight Center, Code 613.1, Building 33, Room A419, Greenbelt, MD 20771, USA.